Journal of Applied Mathematics and Physics, 2025, 13(10), 3393-3430
https://www.scirp.org/journal/jamp
ISSN Online: 2327-4379
ISSN Print: 2327-4352

# Nonlinear Propagation of Coupled Pulses in Birefringent Optical Fibers

**Mathurin Fomekong[1*], Marcelle Nina Zambo Abou'ou[1,2], Oriel Loh Ndichia[1], Jean Roger Bogning[2,3]**

[1]Department of Physics, Faculty of Science, University of Bamenda, Bamenda, Cameroon
[2]African Optical Fiber Family, Camtel Kamkop, Bafoussam, Cameroon
[3]Department of Physics, Higher Teacher Training College, University of Bamenda, Bamenda, Cameroon
Email: *mathurinfomekong@gmail.com

**How to cite this paper:** Fomekong, M., Zambo Abou'ou, M.N., Ndichia, O.L. and Bogning, J.R. (2025) Nonlinear Propagation of Coupled Pulses in Birefringent Optical Fibers. *Journal of Applied Mathematics and Physics*, **13**, 3393-3430.
https://doi.org/10.4236/jamp.2025.1310194

**Received:** August 19, 2025
**Accepted:** October 27, 2025
**Published:** October 30, 2025



## Abstract

The purpose of this work is to study the nonlinear propagation of coupled pulses within birefringent optical fibers. To achieve this, an effective analytical technique using iB-function was applied. With this approach, we decoupled the nonlinear partial differential equations governing the wave propagation and solved them to obtain prototype solutions likely to propagate in the medium. A Mathlab program was then developed to validate the behavior of the propagated waves and analyze the resulting curves. The results revealed distinct complex phenomena such as stable propagation of coupled dark-bright vector soliton, energy exchange between the components during propagation to severe pulse broadening and conditions leading to group velocity walk-off. These findings provided a deeper insight into light propagation, improving its application for advanced optical communication systems and fiber-based devices.

## Keywords

Nonlinear Propagation, Birefringent Optical Fiber, Coupled Pulses, iB-Function, Coupled Nonlinear Partial Differential Equations

## 1. Introduction

Over time, optical fiber has progressively proven itself as the main and leading tool of modern communication. Universally, it has gained the attention of many researchers, as evidenced by the increase in various studies and works in this area [1]-[11]. It provides various possibilities in the field of information transport and signal transmission [12]-[16]. It is also being used more frequently in medicine, particularly in the field of Fibroscopy [17]-[20]. The advantages are multiple in the

industry of new communication technologies. In this work, we align ourselves with the same dynamic to focus on the nonlinear propagation of coupled pulses within birefringent optical fiber. The general observation is that the wave propagation dynamics in optical fibers are often governed by highly complicated nonlinear partial differential equations, which are challenging to solve. While this is true for single-mode optical fiber, it is even more complex in birefringent optical fiber, which has the distinctive characteristic of propagating two signals simultaneously. As light pulses propagate through this fiber, nonlinear interactions can lead to complex phenomena, including pulse shaping, energy exchange, and phase modulation. Recent studies have examined several analytical and numerical approaches to model these relations, providing an understanding of the underlying mechanisms controlling pulse dynamics [21]-[32]. Consequently, the work done in this article consists of the nonlinear propagation of coupled pulses within birefringent optical fiber. All of this involves the outline of a scientific program aimed at facilitating this propagation. Nevertheless, before writing the program, it is essential to first obtain analytical sequences that are solutions to the equations influencing the wave propagation in the birefringent fiber (dispersive and strongly nonlinear coupled Schrödinger equations). Thus, the work initially consists of analytically determining prototype solutions of the coupled partial differential Schrödinger-type equations, using these solutions to initialize the carefully devised numerical program, and subsequently making observations and comments. It should be noted that solving coupled equations, which is crucial to this work, is not easy, especially when using direct integration methods, so the iB-functions were selected along with ansatz solutions to decouple these equations in order to obtain the solutions [32]-[35]. This choice is motivated by the fact that its analytical sequence embodies several types of waves, namely solitary waves and other types of waves and this fact imposes a strong mathematical content. The work here is organized as follows: In Section 2, a brief overview of the iB-functions is provided (methods). Section 3 focuses on seeking signal or prototype solutions. Section 4 contains detailed analysis and comments related to the curves obtained through Mathlab program and at the end of this article, there are reviews of the details of the work performed.

## 2. iB-Functions

### 2.1. Presentation of iB-Functions

iB-functions are versatile mathematical tools with diverse properties, widely applied to solve nonlinear problems in physics and mathematics. These functions exist in two distinct forms: a primary form and a secondary form, with the primary form being hyperbolic form and the secondary form being trigonometric form.

The primary form that will be widely used in this work is defined by

$$J_{n,m}\left(\sum_{i=0}^{p} a_i x_i\right) = \frac{\sinh^m\left(\sum_{i=0}^{p} a_i x_i\right)}{\cosh^n\left(\sum_{i=0}^{p} a_i x_i\right)}, \text{ where } J_{n,m}\left(\sum_{i=0}^{p} a_i x_i\right) \text{ represent the implicit form}$$

of the function, $\sinh^m\left(\sum_{i=0}^{p} a_i x_i\right) \Big/ \cosh^n\left(\sum_{i=0}^{p} a_i x_i\right)$ the explicit form of the function, $a_i\,(i=0,1,2,\cdots,p)$ represent the parameters associated to the independent variable $x_i\,(i=0,1,2,\cdots,p)$, the couple $(n,m)\in R^2$ indicated the power of the function. In a more precise way, $n$ is the power of $\cosh\left(\sum_{i=0}^{p} a_i x_i\right)$ and $m$ is the power of $\sinh\left(\sum_{i=0}^{p} a_i x_i\right)$.

In practice, the iB-function with one variable is mostly used to establish its properties. It is defined by

$$J_{n,m}(\alpha x)=\frac{\sinh^m(\alpha x)}{\cosh^n(\alpha x)}. \tag{1}$$

Equation (1) obeys the transformation

$$J_{n,m}(i\alpha x)=i^m T_{n,m}(\alpha x), \tag{2}$$

where $T_{n,m}(\alpha x)=\dfrac{\sin^m(\alpha x)}{\cos^n(\alpha x)}$, with $i^2=-1$ and $T_{n,m}(\alpha x)$, the secondary form of the iB-function, so called trigonometric form.

## 2.2. Derivatives Properties of the Function $J_{n,m}(\alpha x)$

Common properties of the derivatives include

$$\frac{\mathrm{d}J_{n,m}}{\mathrm{d}x}=m\alpha J_{n-1,m-1}-n\alpha J_{n+1,m+1}, \tag{3}$$

$$\begin{aligned}\frac{\mathrm{d}^2 J_{n,m}}{\mathrm{d}x^2}&=am\left[(m-1)J_{n-2,m-2}-(n-1)J_{n,m}\right]\\&\quad-an\left[(m+1)J_{n,m}-(n+1)J_{n+2,m+2}\right],\end{aligned} \tag{4}$$

If the function $J_{n,m}(\alpha x)$ is a function of single variable, the derivative at other $k$ of $J_{n,m}(\alpha x)$ with the respect to the variable is given by

$$\frac{\mathrm{d}^k J_{n,m}}{\mathrm{d}x^k}=m\alpha\frac{\mathrm{d}^{k-1}J_{n-1,m-1}}{\mathrm{d}x^{k-1}}-n\alpha\frac{\mathrm{d}^{k-1}J_{n+1,m+1}}{\mathrm{d}x^{k-1}}. \tag{5}$$

For the function of parameter $J_{n,m}(\alpha x)$ and independent variable $x$ for the given reals $n,m$ and $p$, we have the following relations:

$$J'_{n+p,m+p}=J'_{2p,2p}J_{n-p,m-p}+J_{2p,2p}J'_{n-p,m-p}, \tag{6}$$

$$J'_{n+p,m+p}J_{n-p,m-p}-J'_{n-p,m-p}J_{n+p,m+p}=J_{2p,2p}J'^2_{n-p,m-p}, \tag{7}$$

and

$$\frac{J'_{2p,2p}}{J_{2p,2p}}=\frac{J'^2_{n-p,m-p}}{J^2_{n-p,m-p}}. \tag{8}$$

## 2.3. Some Properties Linking the Functions $J_{n,m}(ix)$ and $T_{n,m}(x)$

$$J_{2n,2n}(ix)=(-1)^n T_{2n,2n}(x), \tag{9}$$

$$J_{np,mp}(ix) = i^{mp} T_{np,mp}(x), n, m, p \in R \tag{10}$$

and

$$\left|J_{n,m}(ix)\right| = \left|T_{n,m}(x)\right|. \tag{11}$$

### 2.4. Some Usual Transformations

The simple implicit Bogning functions are functions of the form $J_{n,0}$ and $J_{n,1}$, $n \in R$. They are known as simple because, they do not admit any more fractional transformation. Some usual properties of the simple implicit Bogning functions are given as follows:

$$J_{2n+2,2} = J_{2n,0} - J_{2n+2,0}, \tag{12}$$

$$J_{n+3,3} = J_{n+1,1} - J_{n+3,1}, \tag{13}$$

$$J_{2n+3,3} = J_{2n+1,1} - J_{2n+3,1}, \tag{14}$$

$$J_{2n+1,2n+1} = J_{1,1}\left(1 - J_{2,0}\right)^n, \tag{15}$$

and

$$J_{n,m} + J_{n,m}^2 + J_{n,m}^3 + \cdots + J_{n,m}^p = \frac{J_{n,m} - J_{n,m}^{p+1}}{1 - J_{n,m}} = \frac{J_{n,m} - J_{n(p+1),m(p+1)}}{1 - J_{n,m}}. \tag{16}$$

## 3. Forms of Solutions and Solving the Equation

The coupled nonlinear partial differential equations that govern the propagation of solitary waves in birefringent optical fiber is given by

$$\frac{\partial U}{\partial z} + \beta_1 \frac{\partial U}{\partial t} + i\frac{\beta_2}{2}\frac{\partial^2 U}{\partial t^2} + \frac{\alpha_1}{2}U - i\gamma\left(|U|^2 + B|V|^2\right)U = 0, \tag{17}$$

$$\frac{\partial V}{\partial z} + \beta_3 \frac{\partial V}{\partial t} + i\frac{\beta_4}{2}\frac{\partial^2 V}{\partial t^2} + \frac{\alpha_2}{2}V - i\gamma\left(|V|^2 + B|U|^2\right)V = 0, \tag{18}$$

where, $U(z,t)$ and $V(z,t)$ are the envelop of the wave, $\beta_1$ and $\beta_3$ are the coefficients of chromatic dispersion of order one, $\beta_2$ and $\beta_4$ are the coefficients of chromatic dispersion of order two, $\alpha_1$ and $\alpha_2$ are the coefficients of dissipation, $\gamma$ is the coefficient of nonlinearity, $z$ is the spatial variable and $t$ is the time variable.

By using a change of variable $\xi = \alpha z - \alpha_o t$, (19)

$U(z,t)$ and $V(z,t)$ become respectively $U(\xi)$ and $V(\xi)$.

Equations (17) and (18) become respectively,

$$(\alpha - \beta_1\alpha_o)U_\xi + i\frac{\beta_2\alpha_0^2}{2}U_{\xi\xi} + \frac{\alpha_1}{2}U - i\gamma\left(|U|^2 + B|V|^2\right)U = 0, \tag{20}$$

and

$$(\alpha - \beta_3\alpha_o)V_\xi + i\frac{\beta_4\alpha_0^2}{2}V_{\xi\xi} + \frac{\alpha_2}{2}V - i\gamma\left(|V|^2 + B|U|^2\right)V = 0. \tag{21}$$

So, solutions to the above equations will be searched in the form

$$U(\xi)=aJ_{n,m}(\xi), \tag{22}$$

and

$$V(\xi)=bJ_{n,m}(\xi), \tag{23}$$

where, $J_{n,m}(\xi)=\dfrac{\sinh^m(\xi)}{\cosh^n(\xi)}$ is the implicit Bogning function (iBf), $\xi$ represents an independent variable, the pair $(n,m)\in R^2$ indicates the power of the function, $a$ and $b$ are arbitrary non zero constants.

Now, considering Equations (20) and (21) above, we can evaluate the different terms:

$$U_{\xi}=aJ'_{n,m}(\xi), \tag{24}$$

$$U_{\xi\xi}=aJ''_{n,m}(\xi), \tag{25}$$

$$|U|^2=|a|^2J_{2n,2m}(\xi) \tag{26}$$

and

$$|U|^2U=|a|^2aJ_{3n,3m}(\xi). \tag{27}$$

Similarly, we can obtain expressions for $V_{\xi},V_{\xi\xi},|V|^2$ and $|V|^2V$. (28)

### 3.1. Main Equation of Range of Coefficients

Taking into account the ansatz (22) and (23) in Equations (20) and (21) imposes the calculation of its different terms. For this purpose, we obtain after successive derivatives calculations, Equations (29) and (30) below

$$\begin{aligned}&(\alpha-\beta_1\alpha_o)\left[mJ_{n-1,m-1}(\xi)-nJ_{n+1,m+1}(\xi)\right]\\&+i\frac{\beta_2\alpha_0^2}{2}\left[m(m-1)J_{n-2,m-2}(\xi)+n(n+1)J_{n+2,m+2}(\xi)\right.\\&\left.-\left[m(n-1)+n(m+1)\right]J_{(n,m)}(\xi)\right]+\frac{\alpha_1}{2}J_{n,m}(\xi)\\&-i\gamma\left(|a|^2J_{2n,2m}(\xi)+B|b|^2J_{2n',2m'}(\xi)\right)\cdot J_{n,m}(\xi)=0,\end{aligned} \tag{29}$$

and

$$\begin{aligned}&(\alpha-\beta_3\alpha_o)\left[m'J_{n'-1,m'-1}(\xi)-n'J_{n'+1,m'+1}(\xi)\right]\\&+i\frac{\beta_4\alpha_0^2}{2}\left[m'(m'-1)J_{n'-2,m'-2}(\xi)+n'(n'+1)J_{n'+2,m'+2}(\xi)\right.\\&\left.-\left[m'(n'-1)+n'(m'+1)\right]J_{(n',m')}(\xi)\right]+\frac{\alpha_2}{2}J_{n',m'}(\xi)\\&-i\gamma\left(|b|^2J_{2n',2m'}(\xi)+B|a|^2J_{2n,2m}(\xi)\right)J_{n',m'}(\xi)=0.\end{aligned} \tag{30}$$

For $a\neq 0, b\neq 0$, setting $\lambda_1=\alpha-\beta_1\alpha_o, \lambda_2=\dfrac{\beta_2\alpha_0^2}{2}, \lambda_3=\alpha-\beta_3\alpha_o$ and $\lambda_4=\dfrac{\beta_4\alpha_0^2}{2}$,

Equations (29) and (30) are written

$$\begin{aligned}&\lambda_1\left[mJ_{n-1,m-1}(\xi)-nJ_{n+1,m+1}(\xi)\right]\\&+i\lambda_2\left[m(m-1)J_{n-2,m-2}(\xi)+n(n+1)J_{n+2,m+2}(\xi)\right.\\&\left.-\left[m(n-1)+n(m+1)\right]J_{(n,m)}(\xi)\right]+\frac{\alpha_1}{2}J_{n,m}(\xi)\\&-i\gamma\left(|a|^2J_{3n,3m}(\xi)+B|b|^2J_{2n'+n,2m'+m}(\xi)\right)=0,\end{aligned}\tag{31}$$

and

$$\begin{aligned}&\lambda_3\left[m'J_{n'-1,m'-1}(\xi)-n'J_{n'+1,m'+1}(\xi)\right]+\frac{\alpha_2}{2}J_{n',m'}(\xi)\\&+i\lambda_4\left[m'(m'-1)J_{n'-2,m'-2}(\xi)+n'(n'+1)J_{n'+2,m'+2}(\xi)\right.\\&\left.-\left[m'(n'-1)+n'(m'+1)\right]J_{(n',m')}(\xi)\right]\\&-i\gamma|b|^2J_{3n',3m'}(\xi)-i\gamma B|a|^2J_{2n+n',2m+m'}(\xi)=0.\end{aligned}\tag{32}$$

Equations (31) and (32) are the main coefficient range of equations that will be used for the search of all the solutions.

### 3.2. Field of Possible Solutions: Pairs $(n,m)$ and $(n',m')$ for Which Certain Terms of Equations (31) and (32) Can Be Grouped Together

The field of possible solutions of Equations (31) and (32) are given by the values of $n;m;n'$ and $m'$ for which some of their terms are grouped together.

So, we look for the pairs $(n,m)$ and $(n',m')$ such that if $U_iJ_{n,m}$ and $U_jJ_{n',m'}$ are two terms of Equations (31) and (32), we have simultaneously $n=n'$ and $m=m'$, so that

$$\begin{cases}n-1=3n\\m-1=3m\end{cases}\Rightarrow\begin{cases}n=-\frac{1}{2}\\m=-\frac{1}{2}\end{cases}\Rightarrow n=m=-\frac{1}{2},$$

$$\begin{cases}n+1=3n\\m+1=3m\end{cases}\Rightarrow\begin{cases}n=\frac{1}{2}\\m=\frac{1}{2}\end{cases}\Rightarrow n=m=\frac{1}{2},$$

$$\begin{cases}n-2=3n\\m-2=3m\end{cases}\Rightarrow\begin{cases}n=-1\\m=-1\end{cases}\Rightarrow n=m=-1,$$

$$\begin{cases}n+2=3n\\m+2=3m\end{cases}\Rightarrow\begin{cases}n=1\\m=1\end{cases}\Rightarrow n=m=1$$

and

$$\begin{cases}n-1=3n\\m-1=3m\end{cases}\Rightarrow\begin{cases}n=0\\m=0\end{cases}\Rightarrow n=m=0.$$

So, the pairs for which certain terms of Equations (31) and (32) are grouped

together gives fixed couples $(n,m)=(-1,-1),(0,0),(1,1),\left(-\frac{1}{2},-\frac{1}{2}\right)$ and $\left(\frac{1}{2},\frac{1}{2}\right)$. (33)

Similarly, we obtain the fixed couples $(n',m')=(-1,-1),(0,0),(1,1),\left(-\frac{1}{2},-\frac{1}{2}\right)$ and $\left(\frac{1}{2},\frac{1}{2}\right)$. (34)

Apart from the fixed pairs, we obtain constraint relations which link the pairs

$$\begin{cases} n'=n-2 \\ m'=m-2 \end{cases};\begin{cases} n'=n+1 \\ m'=m+1 \end{cases};\begin{cases} n'=n-1 \\ m'=m-1 \end{cases};\begin{cases} n'=n+2 \\ m'=m+2 \end{cases};$$
$$\begin{cases} n'=2n'+n \\ m'=2m'+m \end{cases};\begin{cases} n'=n \\ m'=m \end{cases} \text{ and } \begin{cases} n'=3n \\ m'=3m \end{cases} \quad (35)$$

These relationships above offer good alternatives regarding the resolution of those equations because they establish the links directly between the couples $(n,m)$ and $(n',m')$.

### 3.3. Decoupling Equations (31) and (32) and Resolution

#### 3.3.1. Hyperbolic Solutions

**1) Taking:** $\begin{cases} n=n' \\ m=m \end{cases}$,

then Equations (31) and (32) become respectively

$$\begin{aligned} &\lambda_1\left[mJ_{n-1,m-1}(\xi)-nJ_{n+1,m+1}(\xi)\right] \\ &+i\lambda_2\left[m(m-1)J_{n-2,m-2}(\xi)+n(n+1)J_{n+2,m+2}(\xi)\right. \\ &\left.-\left[m(n-1)+n(m+1)\right]J_{(n,m)}(\xi)\right]+\frac{\alpha_1}{2}J_{n,m}(\xi) \\ &-i\gamma\left(|a|^2J_{3n,3m}(\xi)+B|b|^2J_{3n,3m}(\xi)\right)=0, \end{aligned} \quad (36)$$

and

$$\begin{aligned} &\lambda_3\left[m'J_{n'-1,m'-1}(\xi)-n'J_{n'+1,m'+1}(\xi)\right] \\ &+i\lambda_4\left[m'(m'-1)J_{n'-2,m'-2}(\xi)+n'(n'+1)J_{n'+2,m'+2}(\xi)\right. \\ &\left.-\left[m'(n'-1)+n'(m'+1)\right]J_{(n',m')}(\xi)\right]+\frac{\alpha_2}{2}J_{n',m'}(\xi) \\ &-i\gamma\left(|b|^2J_{3n',3m'}(\xi)+B|a|^2J_{3n',3m'}(\xi)\right)=0. \end{aligned} \quad (37)$$

The values of the pairs for which certain terms of Equations (36) and (37) group together without modifying the structure of Equations (31) and (32) are $(n,m)=(n',m')=(1,1)$ and $(n,m)=(n',m')=(-1,-1)$.

❖ Case 1: $(n,m)=(n',m')=(1,1)$

From Equations (36) and (37), we obtain respectively

$$\begin{aligned} &\lambda_1J_{o,o}(\xi)+\left(\frac{\alpha_1}{2}-2i\lambda_2\right)J_{1,1}(\xi)+\left(2i\lambda_2-i\gamma|a|^2-i\gamma B|b|^2\right)J_{3,3}(\xi) \\ &-\lambda_1J_{2,2}(\xi)=0, \end{aligned} \quad (38)$$

and

$$\lambda_3\left(J_{o,o}(\xi)-J_{2,2}(\xi)\right)+\left(\frac{\alpha_2}{2}-2i\lambda_4\right)J_{1,1}(\xi)+\left(2i\lambda_4-i\gamma|b|^2-i\gamma B|a|^2\right)J_{3,3}(\xi)=0. \tag{39}$$

Using the following relation,

$$J_{3,3}=J_{1,1}\cdot J_{2,2}=J_{1,1}\left(1-J_{2,0}\right)=J_{1,1}-J_{3,1}, \tag{40}$$

Equations (38) and (39) become respectively

$$\lambda_1\left(J_{o,o}(\xi)-J_{2,2}(\xi)\right)+\left(\frac{\alpha_1}{2}-i\gamma|a|^2-i\gamma B|b|^2\right)J_{1,1}(\xi)+\left(2i\lambda_2-i\gamma|a|^2-i\gamma B|b|^2\right)J_{3,1}(\xi)=0, \tag{41}$$

and

$$\lambda_3\left(J_{o,o}(\xi)-J_{2,2}(\xi)\right)+\left(\frac{\alpha_2}{2}-2i\lambda_4\right)J_{1,1}(\xi)+\left(2i\lambda_4-i\gamma|b|^2-i\gamma B|a|^2\right)J_{3,3}(\xi)=0. \tag{42}$$

Equations (41) and (42) are verified if and only if

$$\lambda_1=\lambda_3=0\Rightarrow\beta_1=\beta_3=\frac{\alpha}{\alpha_0}, \tag{43}$$

$$2i\lambda_2-i\gamma|a|^2-i\gamma B|b|^2=0\Rightarrow|a|^2+B|b|^2=\frac{2\lambda_2}{\gamma} \tag{44}$$

and

$$2i\lambda_4-i\gamma|b|^2-i\gamma B|a|^2=0\Rightarrow|b|^2+B|a|^2=\frac{2\lambda_4}{\gamma}. \tag{45}$$

Solving Equations (44) and (45), we obtain the following

$$|a|=\alpha_o\sqrt{\frac{\beta_2-B\beta_4}{\gamma\left(1-B^2\right)}},\gamma\neq0,B\neq1 \tag{46}$$

and

$$|b|=\alpha_o\sqrt{\frac{\beta_4}{\gamma}-\frac{B\left(\beta_2-B\beta_4\right)}{\gamma\left(1-B^2\right)}},\gamma\neq0,B\neq1. \tag{47}$$

Equally,

$$\frac{\alpha_1}{2}-i\gamma|a|^2-i\gamma B|b|^2=0\Rightarrow\frac{\alpha_1}{2}=i\gamma\left(|a|^2+B|b|^2\right), \tag{48}$$

and

$$\frac{\alpha_2}{2}-2i\lambda_4=0\Rightarrow\frac{\alpha_2}{2}=i\gamma\left(|b|^2+B|a|^2\right). \tag{49}$$

Solving Equations (48) and (49), we obtain the following

$$\frac{\alpha_1}{2} = i\alpha_o^2(\beta_2), \tag{50}$$

and

$$\frac{\alpha_2}{2} = i\alpha_o^2(\beta_4). \tag{51}$$

From which, we obtain the following constraints $\alpha_o = \sqrt{\frac{-i\alpha_1}{2\beta_2}}$ and $\alpha = \alpha_o\beta_1$. (52)

Thus, the solution obtained is of the form

$$U(z,t) = \alpha_o\sqrt{\frac{\beta_2 - B\beta_4}{\gamma(1-B^2)}}\exp(i\theta)J_{1,1}(\alpha z - \alpha_o t), \tag{53}$$

and

$$\begin{aligned} &V(z,t) = \alpha_o\sqrt{\frac{\beta_4}{\gamma} - \frac{B(\beta_2 - B\beta_4)}{\gamma(1-B^2)}}\exp(i\theta)J_{1,1}(\alpha z - \alpha_o t), \\ &\text{with } \theta \in \mathbb{R}, \beta_2\cdot\gamma \succ 0, \alpha_o \succ 0, \beta_4\cdot\gamma \succ 0, \alpha_o = \sqrt{\frac{-i\alpha_1}{2\beta_2}} \text{ and } \alpha = \alpha_o\beta_1. \end{aligned} \tag{54}$$

These solutions above are indeed the exact solutions of Equations (31) and (32) when the constraints joining the coefficients of the terms are taken into account such that Equations (17) and (18) become

$$\frac{\partial U}{\partial z} + \frac{\alpha}{\alpha_o}\frac{\partial U}{\partial t} + i\frac{\beta_2}{2}\frac{\partial^2 U}{\partial t^2} + i\alpha_o^2\beta_2 U - i\gamma\left(|U|^2 + B|V|^2\right)U = 0, \tag{55}$$

and

$$\frac{\partial V}{\partial z} + \frac{\alpha}{\alpha_o}\frac{\partial V}{\partial t} + i\frac{\beta_4}{2}\frac{\partial^2 V}{\partial t^2} + i\alpha_o^2\beta_4 V - i\gamma\left(|V|^2 + B|U|^2\right)V = 0. \tag{56}$$

❖ Case 2: $(n,m) = (n',m') = (-1,-1)$

An approach similar to the previous case gives for $(n,m) = (n',m') = (-1,-1)$, the following solutions

$$U(z,t) = \alpha_o\sqrt{\frac{\beta_2 - B\beta_4}{\gamma(1-B^2)}}\exp(i\theta)J_{-1,-1}(\alpha z - \alpha_o t), \tag{57}$$

and

$$\begin{aligned} &V(z,t) = \alpha_o\sqrt{\frac{\beta_4}{\gamma} - \frac{B(\beta_2 - B\beta_4)}{\gamma(1-B^2)}}\exp(i\theta)J_{-1,-1}(\alpha z - \alpha_o t), \\ &\text{with } \theta \in \mathbb{R}, \beta_2\cdot\gamma \succ 0, \alpha_o \succ 0, \beta_4\cdot\gamma \succ 0, \alpha_o = \sqrt{\frac{-i\alpha_1}{2\beta_2}} \text{ and } \alpha = \alpha_o\beta_1. \end{aligned} \tag{58}$$

**2) Taking:** $\begin{cases} n' = n-1 \\ m' = m-1 \end{cases}$ or $\begin{cases} n = n'+1 \\ m = m'+1 \end{cases}$,

then Equations (31) and (32) become respectively

$$\begin{aligned}&\lambda_1\left[mJ_{n-1,m-1}(\xi)-nJ_{n+1,m+1}(\xi)\right]\\&+i\lambda_2\left[m(m-1)J_{n-2,m-2}(\xi)+n(n+1)J_{n+2,m+2}(\xi)\right.\\&\left.-\left[m(n-1)+n(m+1)\right]J_{(n,m)}(\xi)\right]+\frac{\alpha_1}{2}J_{n,m}(\xi)\\&-i\gamma\left(|a|^2J_{3n,3m}(\xi)+B|b|^2J_{3n-2,3m-2}(\xi)\right)=0,\end{aligned}\tag{59}$$

and

$$\begin{aligned}&\lambda_3\left[m'J_{n'-1,m'-1}(\xi)-n'J_{n'+1,m'+1}(\xi)\right]\\&+i\lambda_4\left[m'(m'-1)J_{n'-2,m'-2}(\xi)+n'(n'+1)J_{n'+2,m'+2}(\xi)\right.\\&\left.-\left[m'(n'-1)+n'(m'+1)\right]J_{(n',m')}(\xi)\right]+\frac{\alpha_2}{2}J_{n',m'}(\xi)\\&-i\gamma\left(|b|^2J_{3n',3m'}(\xi)+B|a|^2J_{3n'+2,3m'+2}(\xi)\right)=0.\end{aligned}\tag{60}$$

Equations (59) and (60) are range equations decoupled by the constraint relations $n'=n-1;m'=m-1$. Equation (59) depends exclusively on pairs $(n,m)$ and Equation (60) exclusively on pairs $(n',m')$. Thus, the preponderant pairs $(n,m)$ for which certain terms of Equation (59) are grouped together are $(1,1);(0,0)$ and $\left(\frac{1}{2},\frac{1}{2}\right)$.

Similarly, the leading pairs $(n',m')$ for which certain terms of Equation (60) group together are $(-1,-1);(0,0)$ and $\left(-\frac{1}{2},-\frac{1}{2}\right)$. Our concern is to have two non-trivial solutions and we subsequently search for the solutions for the case $(n,m)=(1,1)\Rightarrow(n',m')=(-1,-1)$.

❖ Case 3: $(n,m)=(1,1)\Rightarrow(n',m')=(-1,-1)$

Equations (59) and (60) give respectively

$$\begin{aligned}&\lambda_1\left(J_{o,o}(\xi)-J_{2,2}(\xi)\right)+\left(\frac{\alpha_1}{2}-2i\lambda_2-i\gamma B|b|^2\right)J_{1,1}(\xi)\\&+\left(2i\lambda_2-i\gamma|a|^2\right)J_{3,3}(\xi)=0,\end{aligned}\tag{61}$$

and

$$\begin{aligned}&\lambda_3J_{o,o}(\xi)-\lambda_3J_{-2,-2}(\xi)+\left(\frac{\alpha_2}{2}-2i\lambda_4-i\gamma B|a|^2\right)J_{-1,-1}(\xi)\\&+\left(2i\lambda_4-i\gamma|b|^2\right)J_{-3,-3}(\xi)=0.\end{aligned}\tag{62}$$

Using the following relation,

$$J_{3,3}=J_{1,1}\cdot J_{2,2}=J_{1,1}\left(1-J_{2,0}\right)=J_{1,1}-J_{3,1},\tag{63}$$

Equations (61) and (62) become respectively

$$\begin{aligned}&\lambda_1\left(J_{o,o}(\xi)-J_{2,2}(\xi)\right)+\left(2i\lambda_2-i\gamma|a|^2\right)J_{3,1}(\xi)\\&+\left(\frac{\alpha_1}{2}-i\gamma|a|^2-i\gamma B|b|^2\right)J_{1,1}(\xi)=0,\end{aligned}\tag{64}$$

and

$$\begin{aligned}&\lambda_3 J_{o,o}(\xi)-\lambda_3 J_{-2,-2}(\xi)+\left(\frac{\alpha_2}{2}-2i\lambda_4-i\gamma B|a|^2\right)J_{-1,-1}(\xi)\\&+\left(2i\lambda_4-i\gamma|b|^2\right)J_{-3,-3}(\xi)=0.\end{aligned}\tag{65}$$

Equations (64) and (65) are verified if and only if $a\neq 0, b\neq 0$, we have the following relations

$$\lambda_1=\lambda_3=0\Rightarrow\beta_1=\beta_3=\frac{\alpha}{\alpha_0},\tag{66}$$

$$2i\lambda_2-i\gamma|a|^2=0\Rightarrow|a|=\alpha_0\sqrt{\frac{\beta_2}{\gamma}},\ \text{that's}\ \ a=\alpha_o\sqrt{\frac{\beta_2}{\gamma}}\exp(i\theta),\beta_2\cdot\gamma\succ 0,\alpha_o\succ 0\tag{67}$$

and

$$2i\lambda_4-i\gamma|b|^2=0\Rightarrow|b|=\alpha_0\sqrt{\frac{\beta_4}{\gamma}},\ \text{that is}\ \ b=\alpha_o\sqrt{\frac{\beta_4}{\gamma}}\exp(i\theta),\beta_4\cdot\gamma\succ 0,\alpha_o\succ 0.\tag{68}$$

Equally,

$$\frac{\alpha_1}{2}-i\gamma|a|^2-i\gamma B|b|^2=0\Rightarrow\frac{\alpha_1}{2}=i\gamma\left(|a|^2+B|b|^2\right),\tag{69}$$

and

$$\frac{\alpha_2}{2}-i\gamma|b|^2-i\gamma B|a|^2=0\Rightarrow\frac{\alpha_2}{2}=i\gamma\left(|b|^2+B|a|^2\right),\tag{70}$$

Solving Equations (69) and (70), we obtain the following

$$\frac{\alpha_1}{2}=i\alpha_o^2(\beta_2+B\beta_4),\tag{71}$$

and

$$\frac{\alpha_2}{2}=i\alpha_o^2(\beta_4+B\beta_2).\tag{72}$$

From which, we obtain the following constraints $\alpha_o=\sqrt{\dfrac{-i\alpha_1}{2(\beta_2+B\beta_4)}}$ and $\alpha=\alpha_o\beta_1$. (73)

Thus, the solutions obtained are of the form

$$U(z,t)=\alpha_o\sqrt{\frac{\beta_2}{\gamma}}\exp(i\theta)J_{1,1}(\alpha z-\alpha_o t),\tag{74}$$

and

$$\begin{aligned}&V(z,t)=\alpha_o\sqrt{\frac{\beta_4}{\gamma}}\exp(i\theta)J_{-1,-1}(\alpha z-\alpha_o t),\beta_2\cdot\gamma\succ 0,\alpha_o\succ 0,\beta_4\cdot\gamma\succ 0\\&\text{with}\ \alpha_o=\sqrt{\frac{-i\alpha_1}{2(\beta_2+B\beta_4)}}\ \text{and}\ \alpha=\alpha_o\beta_1.\end{aligned}\tag{75}$$

These solutions above are indeed the exact solutions of Equations (31) and (32) when the constraints joining the coefficients of the terms are taken into account

such that, Equations (17) and (18) becomes

$$\frac{\partial U}{\partial z}+\frac{\alpha}{\alpha_o}\frac{\partial U}{\partial t}+i\frac{\beta_2}{2}\frac{\partial^2 U}{\partial t^2}+i\alpha_o^2\left(\beta_2+B\beta_4\right)U-i\gamma\left(\left|U\right|^2+B\left|V\right|^2\right)U=0, \tag{76}$$

and

$$\frac{\partial V}{\partial z}+\frac{\alpha}{\alpha_o}\frac{\partial V}{\partial t}+i\frac{\beta_4}{2}\frac{\partial^2 V}{\partial t^2}+i\alpha_o^2\left(\beta_4+B\beta_2\right)V-i\gamma\left(\left|V\right|^2+B\left|U\right|^2\right)V=0. \tag{77}$$

❖ Case 4: $(n,m)=(1,0)\Rightarrow(n',m')=(-1,0)$

Using $(n,m)=(1,0)\Rightarrow(n',m')=(-1,0)$, Equations (59) and (60) give respectively:

$$\begin{aligned}&-\lambda_1 J_{2,1}(\xi)+i\lambda_2\left(2J_{3,2}(\xi)-J_{1,0}(\xi)\right)+\frac{\alpha_1}{2}J_{1,0}(\xi)-i\gamma\left|a\right|^2 J_{3,0}(\xi)\\&-i\gamma B\left|b\right|^2 J_{1,-2}(\xi)=0,\end{aligned} \tag{78}$$

and

$$\lambda_3 J_{0,1}(\xi)+\left(\frac{\alpha_2}{2}+i\lambda_4\right)J_{-1,0}(\xi)-i\gamma\left|b\right|^2 J_{-3,0}(\xi)-i\gamma B\left|a\right|^2 J_{-1,2}(\xi)=0. \tag{79}$$

Considering the transformation $J_{3,2}=J_{1,0}-J_{3,0}$ in Equation (78) above, we obtain:

$$-\lambda_1 J_{2,1}(\xi)-\left(2i\lambda_2+i\gamma\left|a\right|^2\right)J_{3,0}(\xi)+\left(\frac{\alpha_1}{2}+i\lambda_2\right)J_{1,0}(\xi)-i\gamma B\left|b\right|^2 J_{1,-2}(\xi)=0, \tag{80}$$

and

$$\lambda_3 J_{0,1}(\xi)+\left(\frac{\alpha_2}{2}+i\lambda_4\right)J_{-1,0}(\xi)-i\gamma\left|b\right|^2 J_{-3,0}(\xi)-i\gamma B\left|a\right|^2 J_{-1,2}(\xi)=0. \tag{81}$$

Equations (80) and (81) are checked if we have the following relationship

$$\lambda_1=\lambda_3=0\Rightarrow\beta_1=\beta_3=\frac{\alpha}{\alpha_0}, \tag{82}$$

$$\frac{\alpha_1}{2}+i\lambda_2=0\Rightarrow\alpha_1=-i\alpha_o^2\left(\beta_2\right), \tag{83}$$

$$\frac{\alpha_2}{2}+i\lambda_4=0\Rightarrow\alpha_2=-i\alpha_o^2\left(\beta_4\right). \tag{84}$$

From which, we obtain the following constraints $\alpha_o=\sqrt{\frac{i\alpha_1}{\beta_2}}$ and $\alpha=\alpha_o\beta_1$.

(85)

$$i\gamma B\left|b\right|^2=0\Rightarrow\gamma\to 0 \quad \text{since} \quad b\neq 0, \tag{86}$$

$$i\gamma B\left|a\right|^2=0\Rightarrow\gamma\to 0 \quad \text{since} \quad a\neq 0, \tag{87}$$

and

$$2\lambda_2+\gamma\left|a\right|^2=\alpha_o^2\beta_2+\gamma\left|a\right|^2\Rightarrow\left|a\right|^2=-\frac{\alpha_o^2\beta_2}{\gamma}. \tag{88}$$

Finally, we obtain from Equation (88)

$$|a| = \alpha_0 \sqrt{\frac{-\beta_2}{\gamma}}, a = \alpha_o \sqrt{\frac{-\beta_2}{\gamma}} \exp(i\theta), \beta_2 \cdot \gamma \prec 0, \alpha_o \succ 0, \gamma \neq 0, \tag{89}$$

Thus, the solution obtained is of the form

$$\begin{aligned} &U(z,t) = \alpha_o \sqrt{\frac{-\beta_2}{\gamma}} \exp(i\theta) J_{1,0}(\alpha z - \alpha_o t), \\ &\text{with } \theta \in R, \beta_2 \cdot \gamma \prec 0, \alpha_o \succ 0, \alpha_o = \sqrt{\frac{i\alpha_1}{\beta_2}} \text{ and } \alpha = \alpha_o \beta_1. \end{aligned} \tag{90}$$

and

$$V(z,t) = b \exp(i\theta) J_{-1,0}(\alpha z - \alpha_o t), \text{ with } b \neq 0, \tag{91}$$

This solution is indeed the exact solution of Equations (31) and (32), when the constraints joining the coefficients of the terms are taken into account such that (17) and (18) are modified as follows:

$$\frac{\partial U}{\partial z} + \frac{\alpha}{\alpha_o} \frac{\partial U}{\partial t} + i \frac{\beta_2}{2} \frac{\partial^2 U}{\partial t^2} - i\alpha_o^2 \beta_2 U = 0, \tag{92}$$

and

$$\frac{\partial V}{\partial z} + \frac{\alpha}{\alpha_o} \frac{\partial V}{\partial t} + i \frac{\beta_4}{2} \frac{\partial^2 V}{\partial t^2} - i\alpha_o^2 \beta_4 V = 0. \tag{93}$$

The above partial differential equations characterize an optical fiber with weak nonlinearity.

❖ Case 5: $(n,m) = (0,1) \Rightarrow (n',m') = (0,-1)$

Equations (59) and (60) give respectively

$$\lambda_1 J_{-1,0}(\xi) + i\lambda_2 J_{0,1}(\xi) + \frac{\alpha_1}{2} J_{0,1}(\xi) - i\gamma |a|^2 J_{0,3}(\xi) - i\gamma B |b|^2 J_{-2,1}(\xi) = 0, \tag{94}$$

and

$$\begin{aligned} &-\lambda_3 J_{-1,-2}(\xi) + 2i\lambda_4 J_{-2,-3}(\xi) + \frac{\alpha_2}{2} J_{0,-1}(\xi) - i\gamma |b|^2 J_{0,-3}(\xi) \\ &-i\lambda_4 J_{0,-1}(\xi) - i\gamma B |a|^2 J_{2,-1}(\xi) = 0, \end{aligned} \tag{95}$$

Considering the transformation $J_{-2,-3} = J_{0,-3} - J_{0,-1}$ in Equation (95) above, we obtain

$$\lambda_1 J_{-1,0}(\xi) + i\lambda_2 J_{0,1}(\xi) + \frac{\alpha_1}{2} J_{0,1}(\xi) - i\gamma |a|^2 J_{0,3}(\xi) - i\gamma B |b|^2 J_{-2,1}(\xi) = 0, \tag{96}$$

and

$$\begin{aligned} &-\lambda_3 J_{-1,-2}(\xi) + \left(\frac{\alpha_2}{2} - 3i\lambda_4\right) J_{0,-1}(\xi) + \left(2i\lambda_4 - i\gamma |b|^2\right) J_{0,-3}(\xi) \\ &-i\gamma B |a|^2 J_{2,-1}(\xi) = 0. \end{aligned} \tag{97}$$

Equations (96) and (97) are checked if we have the following relationship

$$\lambda_1 = \lambda_3 = 0 \Rightarrow \beta_1 = \beta_3 = \frac{\alpha}{\alpha_0}, \tag{98}$$

$$\frac{\alpha_1}{2} - i\lambda_2 = 0 \Rightarrow \alpha_1 = i\alpha_o^2(\beta_2), \tag{99}$$

$$\frac{\alpha_2}{2} - 3i\lambda_4 = 0 \Rightarrow \alpha_2 = 3i\alpha_o^2(\beta_4). \tag{100}$$

From which, we obtain the following constraints $\alpha_o = \sqrt{\frac{-i\alpha_2}{3\beta_4}}$ and $\alpha = \alpha_o\beta_1$.

(101)

$$i\gamma B|b|^2 = 0 \Rightarrow \gamma \to 0 \quad \text{since} \quad b \neq 0, \tag{102}$$

$$i\gamma B|a|^2 = 0 \Rightarrow \gamma \to 0 \quad \text{since} \quad a \neq 0, \tag{103}$$

and

$$2\lambda_4 - \gamma|b|^2 = \alpha_o^2\beta_4 - \gamma|b|^2 \Rightarrow |b|^2 = \frac{\alpha_o^2\beta_4}{\gamma}. \tag{104}$$

Finally, we obtain from Equation (104)

$$|b| = \alpha_0\sqrt{\frac{\beta_4}{\gamma}}, b = \alpha_o\sqrt{\frac{\beta_4}{\gamma}}\exp(i\theta), \beta_4\cdot\gamma \succ 0, \alpha_o \succ 0, \gamma \neq 0, \tag{105}$$

Thus, the solution obtained is of the form

$$U(z,t) = a\exp(i\theta)J_{0,1}(\alpha z - \alpha_o t), \text{ with } a \neq 0, \tag{106}$$

and

$$\begin{aligned} &V(z,t) = \alpha_o\sqrt{\frac{\beta_4}{\gamma}}\exp(i\theta)J_{0,-1}(\alpha z - \alpha_o t), \\ &\text{with } \theta \in R, \beta_4\cdot\gamma \succ 0, \alpha_o \succ 0, \alpha_o = \sqrt{\frac{-i\alpha_2}{3\beta_4}} \text{ and } \alpha = \alpha_o\beta_1. \end{aligned} \tag{107}$$

This solution is indeed the exact solution of Equations (31) and (32), when the constraints joining the coefficients of the terms are taken into account such that (17) and (18) are modified as follows

$$\frac{\partial U}{\partial z} + \frac{\alpha}{\alpha_o}\frac{\partial U}{\partial t} + i\frac{\beta_2}{2}\frac{\partial^2 U}{\partial t^2} + i\alpha_o^2\beta_2 U = 0, \tag{108}$$

and

$$\frac{\partial V}{\partial z} + \frac{\alpha}{\alpha_o}\frac{\partial V}{\partial t} + i\frac{\beta_4}{2}\frac{\partial^2 V}{\partial t^2} + 3i\alpha_o^2\beta_4 V = 0. \tag{109}$$

The above partial differential equations characterize an optical fiber with weak nonlinearity.

**3) Taking:** $\begin{cases} n' = n+1 \\ m' = m+1 \end{cases}$ or $\begin{cases} n = n'-1 \\ m = m'-1 \end{cases}$,

then Equations (31) and (32) becomes respectively

$$\begin{aligned}&\lambda_1\left[mJ_{n-1,m-1}(\xi)-nJ_{n+1,m+1}(\xi)\right]\\&+i\lambda_2\left[m(m-1)J_{n-2,m-2}(\xi)+n(n+1)J_{n+2,m+2}(\xi)\right.\\&\left.-\left[m(n-1)+n(m+1)\right]J_{(n,m)}(\xi)\right]+\frac{\alpha_1}{2}J_{n,m}(\xi)\\&-i\gamma\left(|a|^2J_{3n,3m}(\xi)+B|b|^2J_{3n+2,3m+2}(\xi)\right)=0\end{aligned}\tag{110}$$

and

$$\begin{aligned}&\lambda_3\left[m'J_{n'-1,m'-1}(\xi)-n'J_{n'+1,m'+1}(\xi)\right]\\&-i\gamma\left(|b|^2J_{3n',3m'}(\xi)+B|a|^2J_{3n'-2,3m'-2}(\xi)\right)+\frac{\alpha_2}{2}J_{n',m'}(\xi)\\&+i\lambda_4\left[m'(m'-1)J_{n'-2,m'-2}(\xi)+n'(n'+1)J_{n'+2,m'+2}(\xi)\right.\\&\left.-\left[m'(n'-1)+n'(m'+1)\right]J_{(n',m')}(\xi)\right]=0.\end{aligned}\tag{111}$$

Equations (110) and (111) are range equations decoupled by the constraint relations $n'=n+1; m'=m+1$. Equation (110) depends exclusively on pairs $(n,m)$ and Equation (111) exclusively on pairs $(n',m')$. Thus, the preponderant pairs $(n,m)$ for which certain terms of Equation (110) are grouped together are $(-1,-1);(0,0)$ and $\left(-\frac{1}{2},-\frac{1}{2}\right)$.

Similarly, the leading pairs $(n',m')$ for which certain terms of Equation (111) group together are $(1,1);(0,0)$ and $\left(\frac{1}{2},\frac{1}{2}\right)$. Our concern is to have two non-trivial solutions, and we subsequently search for the solutions for the case $(n,m)=(-1,-1)\Rightarrow(n',m')=(1,1)$.

❖ Case 6: $(n,m)=(-1,-1)\Rightarrow(n',m')=(1,1)$

Equations (110) and (111) give respectively

$$\begin{aligned}&\lambda_1\left(J_{o,o}(\xi)-J_{-2,-2}(\xi)\right)+\left(\frac{\alpha_1}{2}-2i\lambda_2-i\gamma B|b|^2\right)J_{-1,-1}(\xi)\\&+\left(2i\lambda_2-i\gamma|a|^2\right)J_{-3,-3}(\xi)=0,\end{aligned}\tag{112}$$

and

$$\begin{aligned}&\lambda_3J_{o,o}(\xi)-\lambda_3J_{2,2}(\xi)+\left(\frac{\alpha_2}{2}-2i\lambda_4-i\gamma B|a|^2\right)J_{1,1}(\xi)\\&+\left(2i\lambda_4-i\gamma|b|^2\right)J_{3,3}(\xi)=0.\end{aligned}\tag{113}$$

Using the following relation,

$$J_{3,3}=J_{1,1}\cdot J_{2,2}=J_{1,1}\left(1-J_{2,0}\right)=J_{1,1}-J_{3,1},\tag{114}$$

Equations (112) and (113) become respectively

$$\begin{aligned}&\lambda_1\left(J_{o,o}(\xi)-J_{-2,-2}(\xi)\right)+\left(\frac{\alpha_1}{2}-2i\lambda_2-i\gamma B|b|^2\right)J_{-1,-1}(\xi)\\&+\left(2i\lambda_2-i\gamma|a|^2\right)J_{-3,-3}(\xi)=0,\end{aligned}\tag{115}$$

and

$$\lambda_3 J_{o,o}(\xi) - \lambda_3 J_{2,2}(\xi) + \left(\frac{\alpha_2}{2} - i\gamma|b|^2 - i\gamma B|a|^2\right) J_{1,1}(\xi) - \left(2i\lambda_4 - i\gamma|b|^2\right) J_{3,1}(\xi) = 0. \tag{116}$$

Equations (115) and (116) are verified if and only if $a \neq 0, b \neq 0$, we have the following relations

$$\lambda_1 = \lambda_3 = 0 \Rightarrow \beta_1 = \beta_3 = \frac{\alpha}{\alpha_0}, \tag{117}$$

$$2i\lambda_2 - i\gamma|a|^2 = 0 \Rightarrow |a| = \alpha_0\sqrt{\frac{\beta_2}{\gamma}}, \text{ that's } a = \alpha_o\sqrt{\frac{\beta_2}{\gamma}}e^{i\theta}, \beta_2 \cdot \gamma \succ 0, \alpha_o \succ 0 \tag{118}$$

and

$$2i\lambda_4 - i\gamma|b|^2 = 0 \Rightarrow |b| = \alpha_0\sqrt{\frac{\beta_4}{\gamma}}, \text{ that's } b = \alpha_o\sqrt{\frac{\beta_4}{\gamma}}e^{i\theta}, \beta_4 \cdot \gamma \succ 0, \alpha_o \succ 0. \tag{119}$$

Equally,

$$\frac{\alpha_1}{2} - i\gamma|a|^2 - i\gamma B|b|^2 = 0 \Rightarrow \frac{\alpha_1}{2} = i\gamma\left(|a|^2 + B|b|^2\right), \tag{120}$$

and

$$\frac{\alpha_2}{2} - i\gamma|b|^2 - i\gamma B|a|^2 = 0 \Rightarrow \frac{\alpha_2}{2} = i\gamma\left(|b|^2 + B|a|^2\right), \tag{121}$$

Solving Equations (120) and (121), we obtain the following

$$\frac{\alpha_1}{2} = i\alpha_o^2\left(\beta_2 + B\beta_4\right), \tag{122}$$

and

$$\frac{\alpha_2}{2} = i\alpha_o^2\left(\beta_4 + B\beta_2\right). \tag{123}$$

From which, we obtain the following constraints $\alpha_o = \sqrt{\frac{-i\alpha_1}{2\left(\beta_2 + B\beta_4\right)}}$ and $\alpha = \alpha_o\beta_1$. (124)

Thus, the solutions obtained are of the form

$$U(z,t) = \alpha_o\sqrt{\frac{\beta_2}{\gamma}}\exp(i\theta)J_{-1,-1}(\alpha z - \alpha_o t), \tag{125}$$

and

$$V(z,t) = \alpha_o\sqrt{\frac{\beta_4}{\gamma}}\exp(i\theta)J_{1,1}(\alpha z - \alpha_o t), \beta_2 \cdot \gamma \succ 0, \gamma \neq 0, \alpha_o \succ 0, \beta_4 \cdot \gamma \succ 0$$
$$\text{with } \alpha_o = \sqrt{\frac{-i\alpha_1}{2\left(\beta_2 + B\beta_4\right)}} \text{ and } \alpha = \alpha_o\beta_1. \tag{126}$$

These solutions above are indeed the exact solutions of Equations (31) and (32) when the constraints joining the coefficients of the terms are taken into account

such that, Equations (17) and (18) become

$$\frac{\partial U}{\partial z}+\frac{\alpha}{\alpha_o}\frac{\partial U}{\partial t}+i\frac{\beta_2}{2}\frac{\partial^2 U}{\partial t^2}+i\alpha_o^2\left(\beta_2+B\beta_4\right)U-i\gamma\left(\left|U\right|^2+B\left|V\right|^2\right)U=0, \quad (127)$$

and

$$\frac{\partial V}{\partial z}+\frac{\alpha}{\alpha_o}\frac{\partial V}{\partial t}+i\frac{\beta_4}{2}\frac{\partial^2 V}{\partial t^2}+i\alpha_o^2\left(\beta_4+B\beta_2\right)V-i\gamma\left(\left|V\right|^2+B\left|U\right|^2\right)V=0. \quad (128)$$

### 3.3.2. Other Forms of Solutions: Trigonometric Solutions

One benefit of using iB-functions here is their ability to smoothly convert hyperbolic forms to trigonometric forms. This means we can find corresponding trigonometric solutions by simply mapping $\alpha \leftarrow i\alpha$ and $\alpha_0 \leftarrow i\alpha_0$, such that $i^2=-1$ in our existing solutions.

Since we have many solutions, we'll just show a few examples by using the transformation

$$J_{n,m}\left(ix\right)=i^m T_{n,m}\left(x\right) \quad \text{with} \quad T_{n,m}\left(x\right)=\frac{\sin^m\left(x\right)}{\cos^n\left(x\right)}. \quad (129)$$

**1) Taking:** $\begin{cases} n=n' \\ m=m \end{cases}$,

❖ Case 1: $\left(n,m\right)=\left(n',m'\right)=\left(1,1\right)$

The solution obtained is of the form

$$U\left(z,t\right)=i\alpha_o\sqrt{\frac{\beta_2-B\beta_4}{\gamma\left(1-B^2\right)}}\exp\left(i\theta\right)\tan\left(\alpha z-\alpha_o t\right), B\neq 1, \gamma\neq 0, \quad (130)$$

and

$$V\left(z,t\right)=i\alpha_o\sqrt{\frac{\beta_4}{\gamma}-\frac{B\left(\beta_2-B\beta_4\right)}{\gamma\left(1-B^2\right)}}\exp\left(i\theta\right)\tan\left(\alpha z-\alpha_o t\right), B\neq 1, \gamma\neq 0,$$
$$\text{with } \theta\in\mathbb{R}, \alpha_o\succ 0, \beta_4\cdot\gamma\succ 0, \alpha_o=\sqrt{\frac{-i\alpha_1}{2\beta_2}} \text{ and } \alpha=\alpha_o\beta_1. \quad (131)$$

❖ Case 2: $\left(n,m\right)=\left(n',m'\right)=\left(-1,-1\right)$

The solution obtained is of the form

$$U\left(z,t\right)=-i\alpha_o\sqrt{\frac{\beta_2-B\beta_4}{\gamma\left(1-B^2\right)}}\exp\left(i\theta\right)\operatorname{cotan}\left(\alpha z-\alpha_o t\right), B\neq 1, \gamma\neq 0, \quad (132)$$

and

$$V\left(z,t\right)=-i\alpha_o\sqrt{\frac{\beta_4}{\gamma}-\frac{B\left(\beta_2-B\beta_4\right)}{\gamma\left(1-B^2\right)}}\exp\left(i\theta\right)\operatorname{cotan}\left(\alpha z-\alpha_o t\right),$$
$$\text{with } \theta\in\mathbb{R}, \alpha_o\succ 0, \beta_4\cdot\gamma\succ 0, \alpha_o=\sqrt{\frac{-i\alpha_1}{2\beta_2}} \text{ and } \alpha=\alpha_o\beta_1. \quad (133)$$

**2) Taking:** $\begin{cases} n' = n-1 \\ m' = m-1 \end{cases}$ or $\begin{cases} n = n'+1 \\ m = m'+1 \end{cases}$,

❖ Case 3: $(n,m) = (1,1) \Rightarrow (n',m') = (-1,-1)$

The solutions obtained are of the form

$$U(z,t) = i\alpha_o \sqrt{\frac{\beta_2}{\gamma}} \exp(i\theta) \tan(\alpha z - \alpha_o t), \beta_2 \cdot \gamma \succ 0, \tag{134}$$

and

$$\begin{aligned} &V(z,t) = -i\alpha_o \sqrt{\frac{\beta_4}{\gamma}} \exp(i\theta) \operatorname{cotan}(\alpha z - \alpha_o t), \alpha_o \succ 0, \beta_4 \cdot \gamma \succ 0 \\ &\text{with } \alpha_o = \sqrt{\frac{-i\alpha_1}{2(\beta_2 + B\beta_4)}} \text{ and } \alpha = \alpha_o \beta_1. \end{aligned} \tag{135}$$

❖ Case 4: $(n,m) = (1,0) \Rightarrow (n',m') = (-1,0)$

The solutions obtained are of the form

$$\begin{aligned} &U(z,t) = \alpha_o \sqrt{\frac{-\beta_2}{\gamma}} \exp(i\theta) \sec(\alpha z - \alpha_o t), \\ &\text{with } \theta \in R, \beta_2 \cdot \gamma \prec 0, \alpha_o \succ 0, \alpha_o = \sqrt{\frac{i\alpha_1}{\beta_2}} \text{ and } \alpha = \alpha_o \beta_1. \end{aligned} \tag{136}$$

and

$$V(z,t) = b \exp(i\theta) \cos(\alpha z - \alpha_o t), \text{ with } b \neq 0, \tag{137}$$

❖ Case 5: $(n,m) = (0,1) \Rightarrow (n',m') = (0,-1)$

The solutions obtained are of the form

$$U(z,t) = ia \exp(i\theta) \sin(\alpha z - \alpha_o t), a \neq 0, \text{ with } a \neq 0, \tag{138}$$

and

$$\begin{aligned} &V(z,t) = -i\alpha_o \sqrt{\frac{\beta_4}{\gamma}} \exp(i\theta) \operatorname{cosec}(\alpha z - \alpha_o t), \\ &\text{with } \theta \in R, \beta_4 \cdot \gamma \succ 0, \alpha_o \succ 0, \alpha_o = \sqrt{\frac{-i\alpha_2}{3\beta_4}} \text{ and } \alpha = \alpha_o \beta_1. \end{aligned} \tag{139}$$

**3) Taking:** $\begin{cases} n' = n+1 \\ m' = m+1 \end{cases}$ or $\begin{cases} n = n'-1 \\ m = m'-1 \end{cases}$,

❖ Case 6: $(n,m) = (-1,-1) \Rightarrow (n',m') = (1,1)$

The solutions obtained are of the form

$$U(z,t) = -i\alpha_o \sqrt{\frac{\beta_2}{\gamma}} \exp(i\theta) \operatorname{cotan}(\alpha z - \alpha_o t), \beta_2 \cdot \gamma \succ 0, \tag{140}$$

and

$$\begin{aligned} &V(z,t) = i\alpha_o \sqrt{\frac{\beta_4}{\gamma}} \exp(i\theta) \tan(\alpha z - \alpha_o t), \gamma \neq 0, \alpha_o \succ 0, \beta_4 \cdot \gamma \succ 0 \\ &\text{with } \alpha_o = \sqrt{\frac{-i\alpha_1}{2(\beta_2 + B\beta_4)}} \text{ and } \alpha = \alpha_o \beta_1, \theta \in R. \end{aligned} \tag{141}$$

## 4. Numerical Results and Discussion

For each modification made in the initial birefringent optical fiber, a propagation study to assess the practical feasibility of the solutions obtained is done. But because of the large volume of this work, a few solutions have been chosen to focus on:

■ Case 1: $(n,m)=(n',m')=(1,1)$

The nonlinear coupled partial differential Equations (17) and (18) are decoupled and solved such that the solutions obtained in Equations (53) and (54) can be illustrated, as shown in Figure 1 and Figure 2.

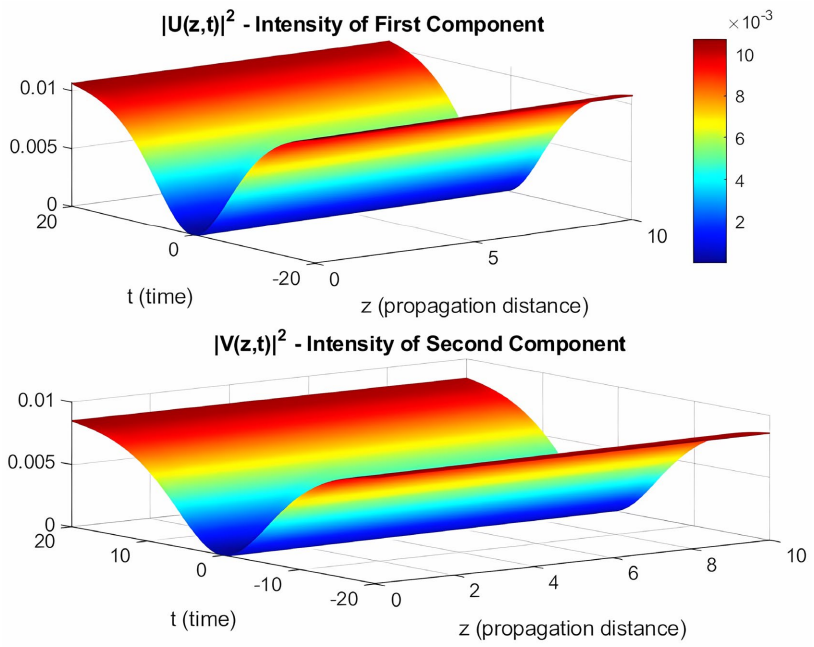


Figure 1. 3D-intensity profiles showing the propagation of coupled pulses $\left|U\left(z,t\right)\right|^2$ and $\left|V\left(z,t\right)\right|^2$, in birefringent optical fibers for the case $\left(n,m\right)=\left(n',m'\right)=\left(1,1\right)$.

**General Observations and Interpretations (Both Profiles):**

- **Axes:** The x-axis represents the propagation distance ($z$) from 0 to 10 units (likely arbitrary units, e.g. meters or kilometers). The y-axis stands for time ($t$) from −20 to 20 units (also arbitrary, e.g. picoseconds or femtoseconds). The z-axis represents the pulse intensity $\left|U\left(z,t\right)\right|^2$ and $\left|V\left(z,t\right)\right|^2$ from 0 to 0.01 (likely arbitrary units, e.g. Watts per metre square or Watts per kilometre square).
- **Color Scale:** Both plots use a heat map where warmer colors (red, yellow) indicate higher intensity and cooler colors (blue) indicate lower intensity. The color bars show the intensity values scaled by $10^{-3}$.
- **Pulse Type:** The plots clearly show a dip in the intensity plot that propagates along the fiber. This is the defining feature of a dark soliton. In contrast, a bright soliton would be a localized intensity peak.
- **Propagation and Stability**: The intensity dips for both components, $U$ and $V$,

maintain their shape and width as they propagate along the z-axis (propagation distance). This stability indicates a balance between nonlinear effects and dispersive effects.

- **Coupling and Birefringence:** The fact that both components show similar periodic temporal variations suggests that they are interacting and influencing each other. This implies that the nonlinear coupling between the two pulses is strong enough to overcome the effects of birefringence, causing them to stick together and propagate.

In summary, the plots demonstrate the successful formation and stable propagation of coupled dark solitons in a birefringent optical fiber. The pulses nonlinear interaction forces them to propagate together as a single unit, despite the fiber's implicit birefringence, focusing on the strong role of nonlinearity in maintaining the pulse structure and order.

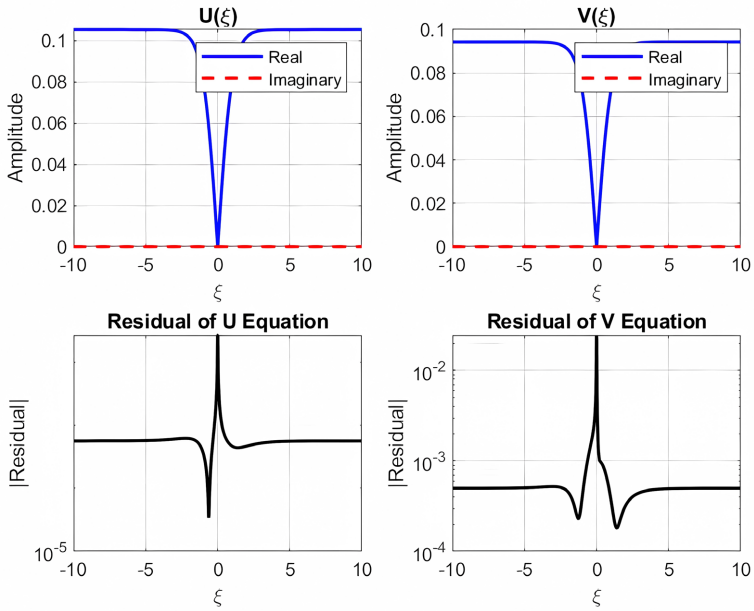


**Figure 2.** Graphs representing the numerical solution of coupled pulses $U(\xi)$ and $V(\xi)$, propagating in birefringent optical fibers, for the case $(n,m)=(n',m')=(1,1)$.

**Observations and Interpretations:**

The first two graphs (horizontally) show the real and imaginary sections of the pulse amplitudes, $U(\xi)$ and $V(\xi)$, while the last two graphs (horizontally) show the residuals of the corresponding equations.

**The Topmost Graphs (horizontally) $U(\xi)$ and $V(\xi)$: Real and Imaginary Sections (Figure 2)**

- **Amplitude Graph:** The blue solid line represents the Real part of $U(\xi)$ and $V(\xi)$ pulses, and it shows a clear "dip" at $\xi=0$, which is a feature of a dark soliton.
- **Imaginary Section:** The red dashed line represents the Imaginary part of $U(\xi)$ and $V(\xi)$ pulses, which is almost zero across the entire range of $\xi$. This indicates that $U(\xi)$ and $V(\xi)$ pulses are predominantly real. As a summary, the fact that

both $U$ and $V$ components display very similar dark soliton graphs with their center at $\xi = 0$ suggests that these are coupled dark solitons that are propagating together without significant walk-off.

**The Lower Graphs (Horizontally): Residual of $U$ and $V$ Equation**

- **Residual Value:** This graph shows the absolute value of the residual of the $U$ and $V$ equations. The residual is a measure of how well the numerical solution solves the underlying differential equation.
- **Spike at $\xi = 0$:** There is a sharp, high spike in the residual at $\xi = 0$, which corresponds strictly to the location of the "dip" in the $U$ and $V$ components. Away from $\xi = 0$, the residual is very low, in the order of $10^{-4}$ to $10^{-3}$.

**Interpretation:** As a result, these plots strongly suggest the numerical investigation of coupled dark solitons propagating in a birefringent optical fiber.

- The fact that their dips are perfectly aligned at $\xi = 0$, confirms that they are coupled and co-propagating. However, the spikes at the soliton center might suggest that, at that particular point the numerical method is not resolving the delicate balance between dispersion and nonlinearity correctly, but the numerical method still struggles with the sharp gradient, high curvature, or rapid change in the wave's properties at that exact location. This does not invalidate the overall accuracy of the solution since the very low (trough) residual away from that "dip" indicates that the numerical solution is highly accurate in those areas.
- The very low imaginary sections suggest that these are fundamental dark solitons, which are typically real or have a constant phase.

■ Case 2: $(n,m) = (n',m') = (-1,-1)$

The nonlinear coupled partial differential Equations (17) and (18) are decoupled and solved such that the solutions obtained in Equations (57) and (58) can be illustrated, as shown in Figure 3 and Figure 4.

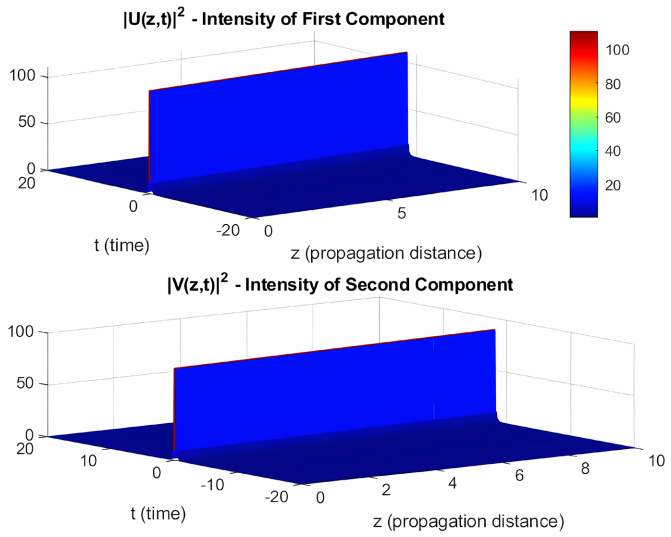


Figure 3. 3D-intensity profiles displaying the propagation of coupled pulses $|U(z,t)|^2$ and $|V(z,t)|^2$, in birefringent optical fibers for the case $(n,m) = (n',m') = (-1,-1)$.

**General Observations and Interpretations (Both Profiles):**

The plots display the intensity profiles of two optical components against propagation distance ($z$) and time ($t$). The x and y-axes are similar to the previous case, while the z-axis ranging from 0 to 100 (likely arbitrary units, e.g. Watts per metre square or Watts per kilometre square), with the color bars showing the intensity values. Both profiles are deep blue, signifying very low or zero intensity everywhere except where the pulses are present.

- **Pulse Trajectory:** There is a single, very thin, bright line (initially red, fading to yellow/green) extending diagonally from approximately ($z = 0$, $t = 0$) to ($z = 10$, $t = 0$, slightly negative value). This diagonal trajectory indicates that the pulse is propagating, and its position in time is changing as it propagates through the fiber.
- **Walk-off/Temporal Shift between Components:** This is the most important observation. While both pulses propagate diagonally, the bright line for $|V(z,t)|^2$ appears to be slightly *displaced* from the bright line for $|U(z,t)|^2$ at any given $z$ meaning that, their group velocities are slightly different, causing a temporal separation as they propagate. This is a strong indicator of group velocity walk-off. Walk-off can be a serious issue in optical communication systems, leading to pulse broadening, if not properly managed.
- **No Strong Coupling/Interaction:** Unlike the previous case, where the pulses maintained a tight bond and, periodic structure, here they appear to be propagating more independently, with their relative temporal positions changing.

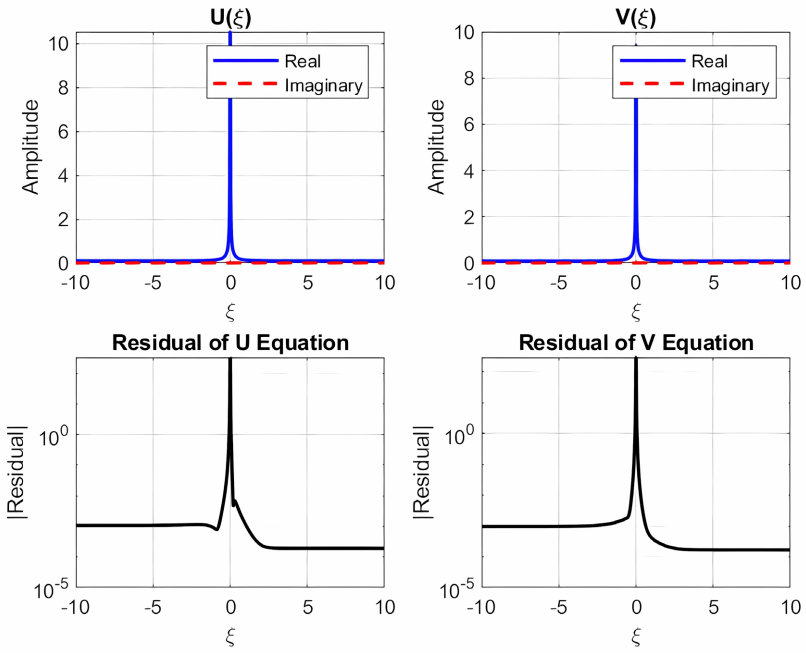


**Figure 4.** Graphs representing the numerical solution of coupled pulses $U(\xi)$ and $V(\xi)$, propagating in birefringent optical fibers, for the case $(n,m)=(n',m')=(-1,-1)$.

As a summary, the above profiles indicate the propagation of two distinct, lo-

calized pulses through a birefringent optical fiber with no strong coupling due to their relative temporal position changing. The most prominent feature here is the group velocity walk-off between the two coupled components, where they gradually separate in time as they propagate along the fiber. Walk-off can be a significant issue in optical communication systems, leading to pulse broadening, if not properly managed.

**Observations and Interpretations (Figure 4):**

The top two graphs (first row) show the real and imaginary sections of the pulse amplitudes, $U(\xi)$ and $V(\xi)$, while the bottom two graphs (second row) show the residuals of the corresponding equations.

**The Graphs on the First Row $U(\xi)$ and $V(\xi)$: Real and Imaginary Sections**

- **Amplitude Plot:** The blue solid line (Real part of $U$ and $V$) shows a prominent, sharp peak centered at $\xi = 0$. The amplitude rises significantly from a near-zero background, reaching a peak value. This shape is typical of a bright soliton.
- **Imaginary Section:** The red dashed line (Imaginary part of $U$ and $V$) is practically zero across the entire range of $\xi$. This indicates that the $U$ and $V$ components are mainly real, or their imaginary part is negligible in magnitude compared to the real part.

In summary, the fact that both $U$ and $V$ components display very similar bright soliton profiles and are perfectly centered at $\xi = 0$ indicates that these are coupled bright solitons that are propagating together without significant walk-off.

**The Graphs on the Second Row: Residual of $U$ and $V$ Equation**

- **Residual Value:** These graphs show the absolute value of the residual of the $U$ and $V$ equations on a logarithmic scale.
- **Spike at $\xi = 0$:** There is a very sharp and high spike in the residual at $\xi = 0$, which matches precisely to the peak of the bright soliton. Away from $\xi = 0$, the residual rapidly drops to extremely low values, on the order of $10^{-5}$.

In brief, the exceptionally low residual away from the peak indicates that the numerical solution is highly accurate in the "tails" of the pulse. The significant spike at $\xi = 0$ implies that the numerical method faces challenges in accurately capturing the rapid changes in amplitude.

Overall, these graphs indicate firmly the numerical investigation of coupled bright solitons propagating in a birefringent optical fiber.

- The negligible imaginary parts reinforce the idea that these are fundamental bright solitons, which are often described by real functions (or can be rotated to be real).
- The residual graphs effectively bring out the regions where the numerical solution deviates most from the exact solution due to the inherent difficulty in precisely resolving very sharp features, such as the peak of a bright soliton. The overall extremely low residuals away from the peak suggest a good quality numerical solution.

■ Case 3: $(n,m) = (1,1) \Rightarrow (n',m') = (-1,-1)$

The nonlinear coupled partial differential Equations (17) and (18) are decoupled and solved such that the solutions obtained in Equations (74) and (75) can be drawn, as shown in Figure 5 and Figure 6.

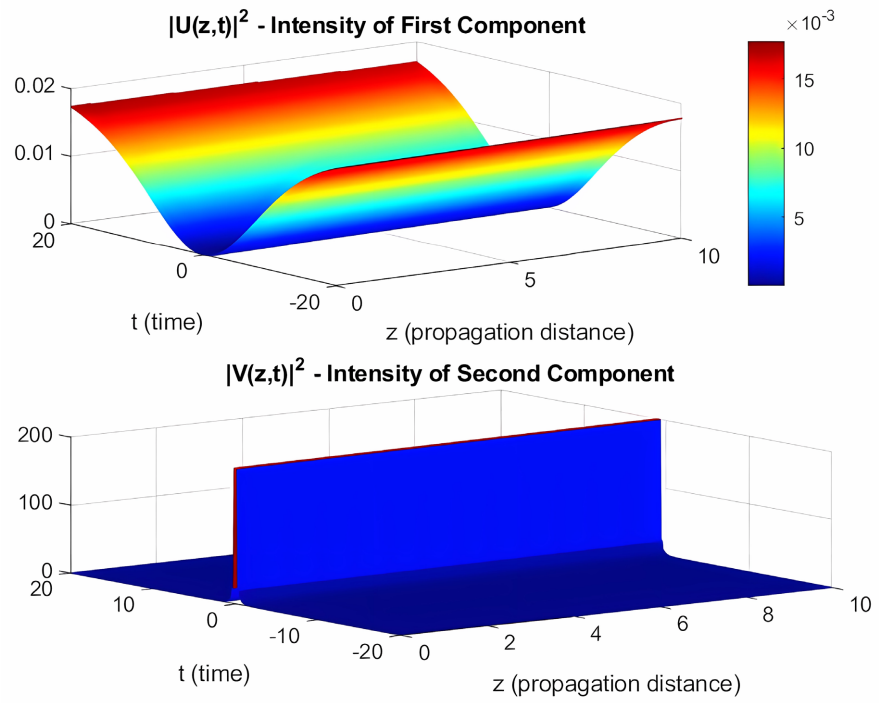


Figure 5. Intensity profiles displaying the propagation of coupled pulses $|U(z,t)|^2$ and $|V(z,t)|^2$, in birefringent optical fibers for the case $(n,m)=(1,1)\Rightarrow(n',m')=(-1,-1)$.

**General Observations and Interpretations (Both Profiles):**

- **Axes:** The x-axis stand for propagation distance ($z$) from 0 to 10 units, the y-axis stands for time ($t$) from −20 to 20 units and The z-axis represents the pulse intensity $|U(z,t)|^2$ and $|V(z,t)|^2$ from 0 to 200 (likely arbitrary units, e.g. Watts per metre square or Watts per kilometre square).
- **Color Scale:** Both charts use a heat map, but their intensity ranges and color bar values are immensely different.
- **Asymmetric Power Distribution:** The second component, $|V(z,t)|^2$ carries exceptionally more power(intensity) than the first component $|U(z,t)|^2$ (see the scale). This suggests an uneven distribution of energy between the two polarizations or modes.
- **Different Propagation Regimes:** Each component appears to be in a different propagation regime:

- **First Component ($|U(z,t)|^2$):** Behaves like a periodically modulated continuous wave or a train of exceedingly low-intensity pulses compared to the second component.
- **Second Component ($|V(z,t)|^2$):** Behaves like a single, high-intensity, stable

pulse. This could represent a fundamental soliton or a highly localized bright pulse, where nonlinearity perfectly balances dispersion for this component.

In summary, this set of charts illustrates a compelling case of a highly asymmetric and distinct reaction between the two components, propagating in birefringent optical fiber. A very high-intensity, localized second component appears to propagate stably, while a much weaker first component displays a strong periodic temporal transformation, likely induced by nonlinear interactions with the dominant first component. There is an absence of a significant temporal walk-off between the two components, despite the birefringence.

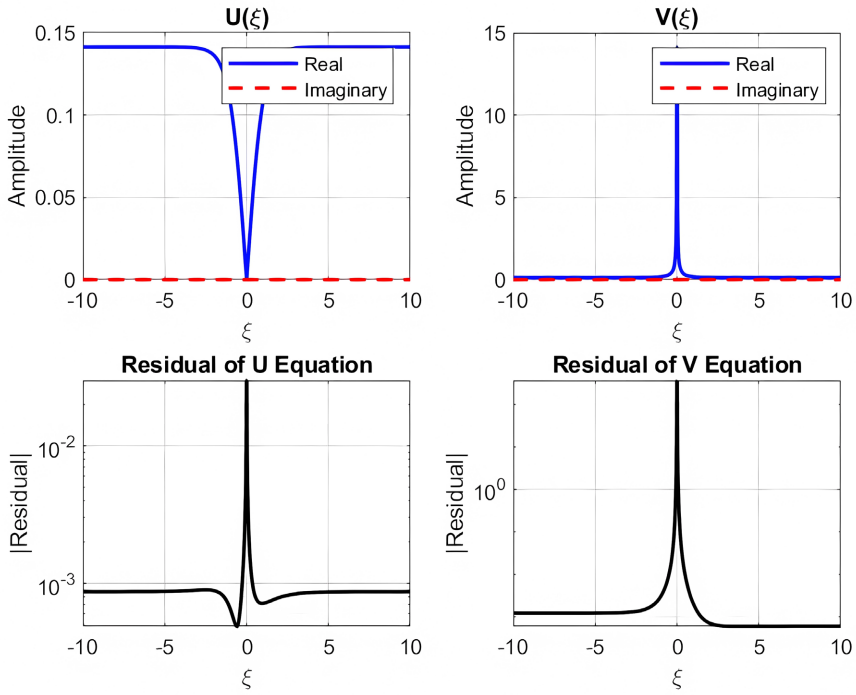


**Figure 6.** Graphs representing the numerical solution of coupled pulses $U(\xi)$ and $V(\xi)$, propagating in birefringent optical fibers, for the case $(n,m)=(1,1)\Rightarrow(n',m')=(-1,-1)$.

**Observations and Interpretations:**

**The Graphs (Top Row) $U(\xi)$ and $V(\xi)$: Real and Imaginary Sections**

This case is particularly intriguing as it combines features of both dark and bright solitons, showing a mixed-type coupled solution.

- **Amplitude Plot:** The blue solid line (Real part of $U$) shows a clear "dip" at $\xi=0$, while that of $V$ (Real part of $V$) shows a prominent, sharp peak centered at $\xi=0$. These show that, the first component ($U$) displays the characteristic "dark" profile, while the other component ($V$) displays the characteristic "bright" profile.
- **Imaginary Section:** The red dashed line (Imaginary part of $U$ and $V$) is virtually zero across the entire range of $\xi$. This indicates that the $U$ and $V$ component are predominantly real, meaning that their imaginary sections are negligible in magnitude compared to the real part.

**The Graphs (Bottom Row): Residual of U and V Equation**

- **Residual Value:** This graph shows the absolute value of the residual of the $U$ and $V$ equations on a logarithmic scale.
- **Spike at $\xi = 0$:** There is a sharp spike in the residual at $\xi = 0$, which matches precisely to the location of the "dip" in the $U$ component, while that of $V$ shows a very sharp and high spike in the residual at $\xi = 0$, aligning with the peak of the bright soliton.

**Interpretation:** The very low residual away from the "dip" indicates that the numerical solution is highly accurate in those regions. The observations and interpretations for the $V$ equation's residual are similar to those for bright solitons in previous cases. The overall extremely low residuals away from the peak suggest a good quality numerical solution for this component as well.

As a summary, these graphs strongly demonstrate the numerical investigation of mixed-type coupled solitons (specifically, a coupled dark-bright soliton pair) propagating in birefringent optical fiber.

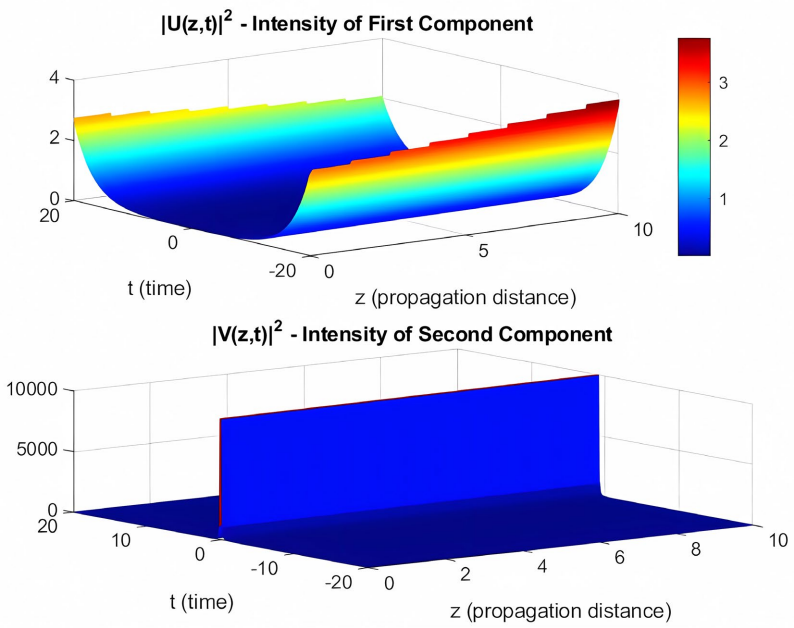


**Figure 7.** Intensity profiles displaying the propagation of coupled pulses $|U(z,t)|^2$ and $|V(z,t)|^2$, in birefringent optical fibers for the case $(n,m)=(1,0) \Rightarrow (n',m')=(-1,0)$.

- Their perfect pattern and arrangement (both centered at $\xi = 0$) are crucial. This means that they are propagating together as a stable bound state, often referred to as a dark-bright vector soliton. This type of solution can arise when the coupling mechanism leads to this mixed-type solution.
- The minor imaginary parts for both components suggest that these are fundamental dark and bright solitons, which can often be described by real functions.
- The residual plots effectively point out the numerical challenges in precisely

resolving the sharp features essential in both dark (dip) and bright (peak) soliton solutions. Despite these localized spikes, the extremely low residuals elsewhere suggest that the numerical method provides a good estimate of these complex coupled solutions.

This case is a typical example of how different types of solitons can be coupled and propagate together in birefringent media, showcasing the infinite variety of nonlinear phenomena in optical fibers.

■ Case 4: $(n,m)=(1,0)\Rightarrow(n',m')=(-1,0)$

The nonlinear coupled partial differential Equations (17) and (18) are decoupled and solved such that the solutions obtained in system Equations (90) and (91) can be drawn, as shown in Figure 7 and Figure 8.

**General Observations and Interpretation (Both Profiles):**

❖ **Extreme Power Asymmetry:** The most striking feature is the wide difference in peak intensity between the two components. The second component is several orders of magnitude more intense than the first component (see scale). This suggests that almost all the power is concentrated in one polarization (or mode).

❖ **Dominant Pulse and Weak Background:** The second component ($|V(z,t)|^2$) appears to be propagating as an extremely stable, high-intensity fundamental soliton.

❖ **Effective Single-Component Propagation:** Given the broad intensity difference, this case is practically similar to the propagation of a single, very strong pulse (the second component) in a fiber, with the first component being negligible or effectively decoupled from the dynamics of the main pulse.

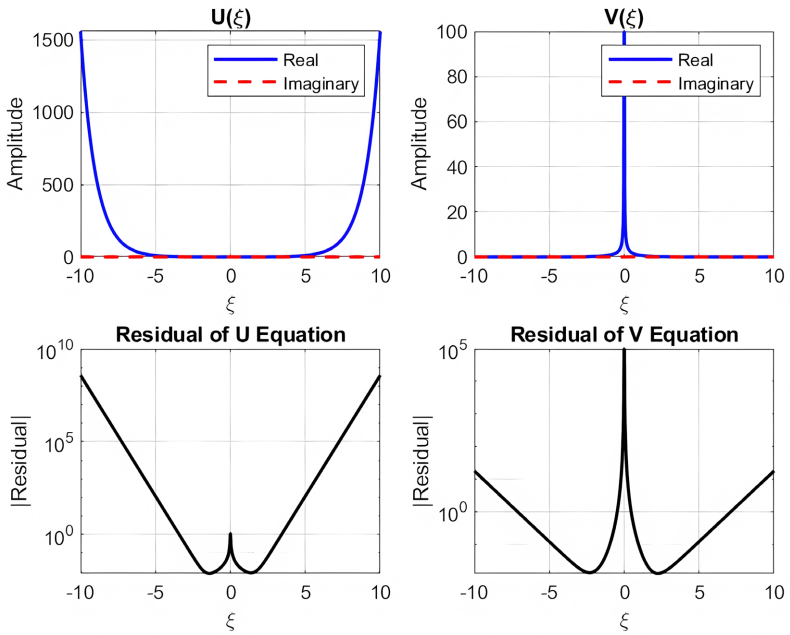


Figure 8. Graphs representing the numerical solution of coupled pulses $U(\xi)$ and $V(\xi)$, propagating in birefringent optical fibers, for the case $(n,m)=(1,0)\Rightarrow(n',m')=(-1,0)$.

As a summary, this case demonstrates a highly uneven coupled pulse propagation where one component ($|V(z,t)|^2$) is dominant in intensity and propagates as a remarkably stable, localized pulse, probably a fundamental soliton. The other component ($|U(z,t)|^2$) exists as a very weak, diffused, and likely dispersive background, with minimal visible interaction or influence from the dominant pulse. This setup effectively reduces the coupled system to the propagation of a single, powerful pulse in a birefringent fiber, with negligible involvement from the orthogonal polarization.

**Observations and Interpretations:**

**The Graphs (Top Row) $U(\xi)$ and $V(\xi)$: Real and Imaginary Sections**

- **Amplitude Graph:** The blue solid line (Real part of $U$ and $V$) shows a profile with very high amplitudes at the boundaries of the $\xi$ range (around 1500) and a significant dip towards a low value (near zero) in the center. There are also minute peaks or oscillations near $\xi = 0$. This pattern, with high amplitude at the edges and a dip in the middle, is characteristic of a higher-order dark soliton or a dark-dark soliton bound state.
- **Imaginary Sections:** The red dashed line (Imaginary part of $U$) is essentially zero across the entire range of $\xi$, indicating that the $U$ component is predominantly real.

**The Graph (Bottom Row): Residual of $U$ and $V$ Equation**

- **Residual Value:** This plot shows the absolute value of the residual of the $U$ and $V$ equations on a logarithmic scale.
- **Spike at $\xi = 0$:** There is an exceptionally sharp and high spike in the residual (around 105) at $\xi = 0$, corresponding to the peak of the bright soliton.
- **High Residuals at Edges and Spikes:** Common for dark solitons, indicating numerical challenges in resolving sharp features or rapid changes in derivative.

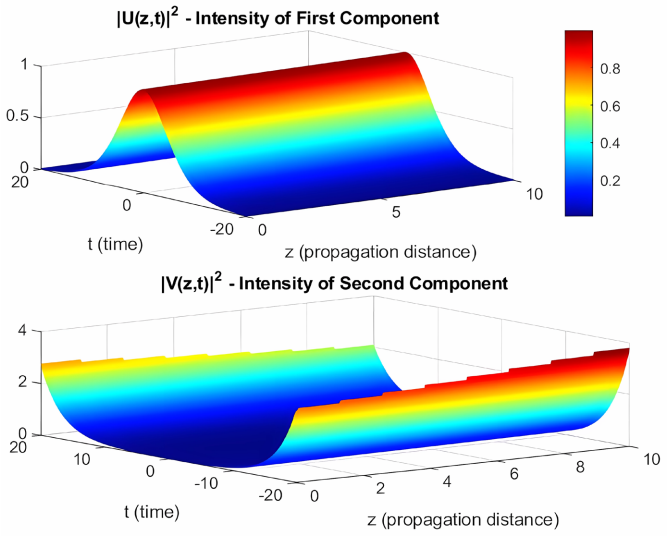


**Figure 9.** Intensity profiles displaying the propagation of coupled pulses $|U(z,t)|^2$ and $|V(z,t)|^2$, in birefringent optical fibers for the case $(n,m)=(0,1) \Rightarrow (n',m')=(0,-1)$.

In summary, these plots reveal a complex framework of mixed-type coupled solitons, specifically a higher-order dark soliton coupled with a bright soliton. The $U$ component forms an extended dark-type structure, while the $V$ component is a localized bright pulse. Their perfect arrangement at $\xi = 0$ is a distinctive feature of dark-bright vector solitons or more complex coupled structures. The presence of these higher residuals suggests that while a solution has been found, its numerical accuracy might be limited in certain areas, possibly due to the intricate nature of the solution itself.

■ Case 5: $(n,m) = (0,1) \Rightarrow (n',m') = (0,-1)$

The nonlinear coupled partial differential Equations (17) and (18) are decoupled and solved such that the solutions obtained in Equations (106) and (107) can be illustrated, as shown in Figure 9 and Figure 10.

**General Observations and Interpretation (Both Profiles):**

- **Dominant Second Component:** The second component ($\left|V(z,t)\right|^2$) is obviously the dominant one in terms of intensity and seems to propagate in a stable and broad pulse manner. (See scale.)
- **Negligible First Component:** The first component ($\left|U(z,t)\right|^2$) is extremely weak and seems to be a mere background or a highly weakened/dispersed pulse. Its presence is almost negligible in the overall dynamics.
- **Effective Single-Polarization Propagation:** Similar to Case 4, this scenario effectively reduces to the propagation of a single, dominant component (the second one) in a birefringent fiber.
- **Birefringence without Visible Effect:** While the fiber is birefringent, its effect (like walk-off) is not clearly manifested between the two components because one component is dominant and wide, while the other is too weak to exhibit clear pulse dynamics or interactions.

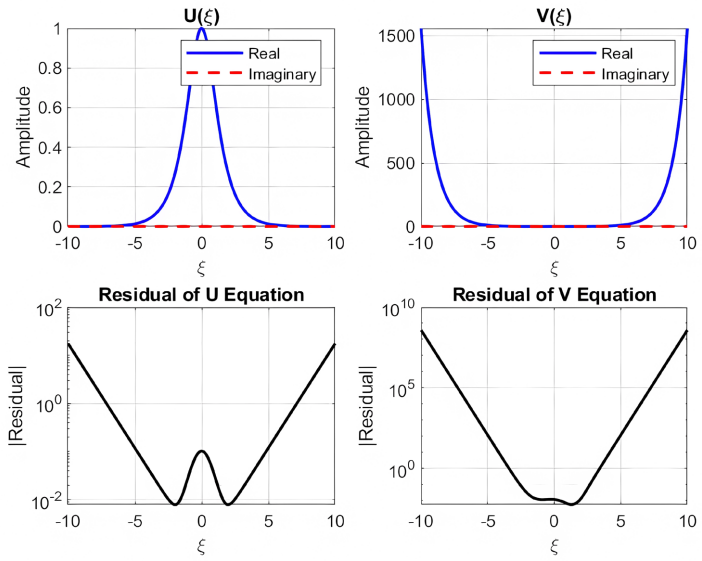


Figure 10. Graphs representing the numerical solution of coupled pulses $U(\xi)$ and $V(\xi)$, propagating in birefringent optical fibers, for the case $(n,m) = (0,1) \Rightarrow (n',m') = (0,-1)$.

- **Possible Input Conditions:** This might arise from input conditions where almost all the optical power is launched into one polarization state (the second component), with very little power in the orthogonal state (the first component).

As a summary, these plots illustrate a structure where one of the coupled pulse components ($|V(z,t)|^2$) is significantly dominant in intensity, propagating as a wide and stable pulse. The first component ($|U(z,t)|^2$) is extremely weak and appears as a negligible background, possibly declining.

**Observations and Interpretations:**

**The Top Graph (First Row) $U(\xi)$ and $V(\xi)$: Real and Imaginary Sections**

- **Amplitude Plot:** The blue solid line (Real part of $U$) shows a single, sharp, bell-shaped peak centered at $\xi = 0$, reaching an amplitude of approximately 0.9. This is typical of a bright soliton, while that of $V$ is significantly dipped towards zero in the center, with small peaks or oscillations near $\xi = 0$. This is habitual of a higher-order dark soliton.
- **Imaginary Section:** The red dashed line (Imaginary part of $U$ and $V$) is more or less zero across the entire range of $\xi$, indicating that the $U$ and $V$ components are mostly real.

**The Bottom Graph (Second Row): Residual of $U$ and $V$ Equation**

- The spike at $\xi = 0$, for $U$ indicates numerical difficulty in resolving the sharp peak, as commonly seen with bright solitons, while the very low residual away from the peak indicates good numerical accuracy in the tails.
- The extremely high residuals at the edges suggest problems with boundary conditions or the numerical method for extended dark structures. The spikes near the central dips are typical of dark solitons.

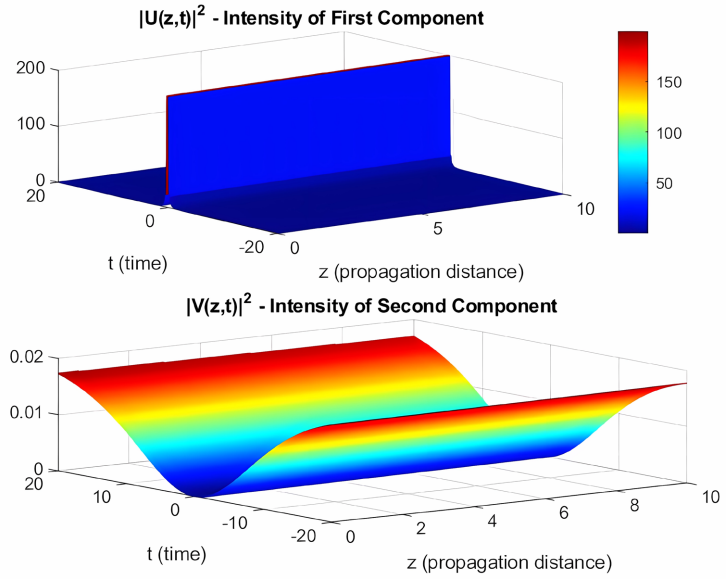


**Figure 11.** Intensity profiles displaying the propagation of coupled pulses $|U(z,t)|^2$ and $|V(z,t)|^2$, in birefringent optical fibers for the case $(n,m)=(-1,-1) \Rightarrow (n',m')=(1,1)$.

As a result, this case demonstrates a mixed-type coupled soliton solution, where the $U$ component is a bright soliton and the $V$ component is a higher-order dark soliton (or dark-dark bound state). Their coordination at $\xi = 0$ is crucial, indicating a stable bound state, a form of dark-bright vector soliton. The very high residuals, particularly for the $V$ component, emphasize the significant numerical challenges in accurately representing this complex coupled system, especially for the extended dark structure.

■ Case 6: $(n,m) = (-1,-1) \Rightarrow (n',m') = (1,1)$

The nonlinear coupled partial differential Equations (17) and (18) are decoupled and solved such that the solutions obtained in Equations (125) and (126) can be plotted, as shown in Figure 11 and Figure 12.

**General Observations and Interpretation (Both Profiles):**

This case shows a riveting inversion of the asymmetric behaviour seen in Case 3.

❖ **Intensity Range:** The intensity of the first component is relatively high, ranging from approximately 0 to 150, while that of the second component is significantly lower, ranging from approximately 0 to $15 \times 10^{-3}$ (or 0.015).

❖ **Inverted Power Asymmetry:** This case is essentially an inversion of Case 3, where the roles of the dominant and modulated components are interchanged. Here, the first component ($|U|^2$) is the high-intensity, localized pulse, while the second component ($|V|^2$) is the much weaker, periodically modulated wave.

❖ **Cross-Polarization Coupling with Energy Transfer/Modulation:** The coexistence of these two immensely different behaviours, coupled with the stability of both patterns along $z$, strongly suggests complex nonlinear interactions, the first strong component could be acting as a "pump" or "driver" for the second component.

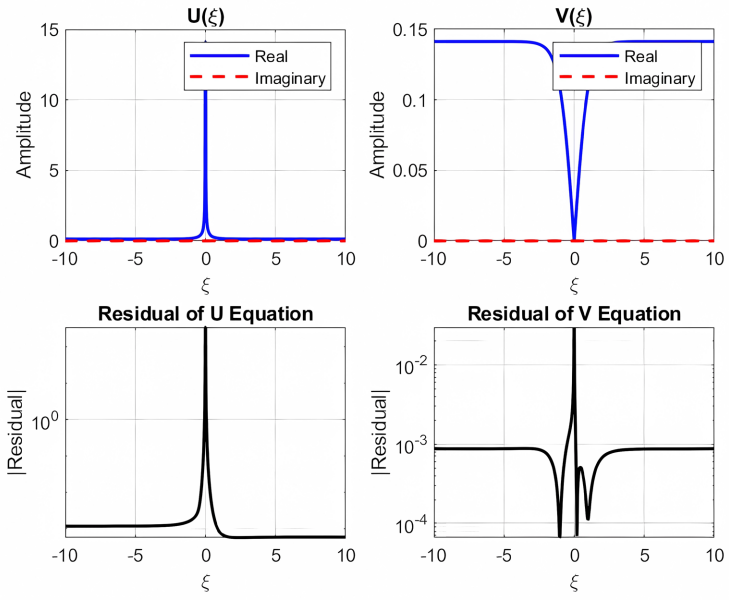


Figure 12. Graphs representing the numerical solution of coupled pulses $U(\xi)$ and $V(\xi)$, propagating in birefringent optical fibers, for the case $(n,m) = (-1,-1) \Rightarrow (n',m') = (1,1)$.

- **No Apparent Walk-off Between Components:** Despite the birefringent nature of the fiber, there is no noticeable temporal walk-off between the two components. The highly localized first component remains centered, and the modulated second component also seems to maintain its overall periodic pattern without shifting relative to the first component.

In summary, these plots illustrate a compelling case of highly asymmetric coupled pulse propagation in a birefringent fiber, where a very high-intensity, localized first component propagates stably, while a much weaker second component displays strong periodic temporal modulation.

**Observations and Interpretations:**

**The Top Graphs (First Row) $U(\xi)$ and $V(\xi)$: Real and Imaginary Sections**

- **Amplitude Graph:** The blue solid line (Real part of $U$) shows a single, sharp, bell-shaped peak centered at $\xi = 0$, reaching an amplitude of approximately $10^{-12}$. This is common in a bright soliton, while that of $V$ shows a clear dip at $\xi = 0$. This plot is familiar with a dark soliton or a dark-like solution.
- **Imaginary Section**: The red dashed line (Imaginary part of $U$ and $V$) is approximately zero across the entire range of $\xi$, indicating that the $U$ and $V$ components are predominantly real.

**The Bottom Graphs (Second Row): Residual of $U$ and $V$ Equation**

- There is a very sharp and high spike in the residual for $U$ (around 100 to 101) at $\xi = 0$, corresponding to the peak of the bright soliton, while that of $V$ shows a sharp spike (around 100 to 101) at $\xi = 0$, corresponding to the dip of the dark soliton. Very low residual away from the peak indicates good numerical accuracy.

In summary, these diagrams describe a mixed-type coupled soliton solution, specifically a bright-dark vector soliton. The $U$ component is a bright soliton, and the $V$ component is a dark soliton. Their precise layout and concordance at $\xi = 0$ confirm that they form a stable bound state. The residual plots highlight the numerical challenges in accurately resolving the sharp features of both bright and dark solitons.

Across the six cases studied in the course of this work, we collectively obtained twelve figures, where **Figure 1**, **Figure 3**, **Figure 5**, **Figure 7**, **Figure 9** and **Figure 11** represent the intensities of the envelopes of the coupled signals resulting from the solutions obtained and **Figure 2**, **Figure 4**, **Figure 6**, **Figure 8**, **Figure 10** and **Figure 12** representing the graphs of the corresponding residuals equations. Under Case 1, we have **Figure 1**, which shows the stable co-propagation of two coupled dark solitons in a birefringent fiber and **Figure 2**, confirming the existence of two coupled dark solitons by showing their real parts as dips at the same point, with negligible imaginary parts and low residuals. As for Case 2, **Figure 3** displays two distinct pulses propagating diagonally with a visible temporal separation (walk-off), indicating weak or no strong coupling and **Figure 4**, showing the numerical solution of two coupled bright solitons centered at the same point, with negligible imaginary parts and low residuals everywhere except at the central peak. In Case

3, Figure 5 illustrates a highly asymmetric propagation, where a dominant, stable, high-intensity pulse coexists with a much weaker, periodically modulated wave without walk-off and Figure 6, presenting a mixed-type coupled solution, showing one component as a bright soliton and the other as a dark soliton propagating together. As for Case 4, Figure 7 demonstrates an extreme power asymmetry where one component is a very stable, dominant pulse, while the other is a weak, negligible background and Figure 8 reveals a complex mixed-type solution where a higher-order dark soliton is coupled with a bright soliton, forming a stable bound state. For Case 5, Figure 9 illustrates a highly asymmetric case where one component is a stable, dominant pulse, and the other is an extremely weak, negligible background and Figure 10 confirms a mixed-type coupled soliton, with a bright soliton and a higher-order dark soliton forming a stable bound state. And therefore, Case 6 with Figure 11 shows a high-intensity, stable pulse coupled with a much weaker, periodically modulated component, similar to Case 3 but with the roles of the two components inverted and Figure 12 depicts a bright-dark vector soliton solution where one component is a bright soliton and the other is a dark soliton, forming a stable bound state.

## Parametric Studies: Effect of Birefringence Parameters on Soliton Separation

A parametric study shows the effect of birefringence parameters on soliton behaviour (Table 1).

Table 1. Effect of birefringence parameters on soliton separation.

| Beta1-parameter | *B*-parameter | Max *U*-*V* Separation |
|---|---|---|
| 0.08 | 0.6 | 0.750 |
| 0.08 | 0.8 | 0.667 |
| 0.08 | 1.0 | 0.600 |
| 0.10 | 0.6 | 0.625 |
| 0.10 | 0.8 | 0.556 |
| 0.10 | 1.0 | 0.500 |
| 0.12 | 0.6 | 0.500 |
| 0.12 | 0.8 | 0.444 |
| 0.12 | 1.0 | 0.400 |

❖ $\beta_1$ **(Linear Birefringence Parameter):**

This parameter represents the linear birefringence of the optical fiber. It quantifies the difference in group velocities between the two polarization components ($U$ and $V$). The values for beta1 in the table are 0.08, 0.10, and 0.12. As beta1 increases (e.g., from 0.08 to 0.12) while $B$ is kept constant, the Max $U$-$V$ Separation *decreases*. For instance, when $B$ is 0.6, increasing beta1 from 0.08 to 0.12 causes the separation to drop from 0.750 to 0.500. This suggests that a stronger linear birefringence might lead to a smaller maximum separation of the solitons.

❖ ***B*** **(Cross-Phase Modulation Parameter):**

This parameter represents the strength of cross-phase modulation (XPM) between the $U$ and $V$ polarization components. XPM describes how the phase of one component is affected by the intensity of the other. The values for $B$ in the table are 0.6, 0.8, and 1.0. As $B$ increases (e.g., from 0.6 to 1.0) while beta1 is kept constant, the Max $U$-$V$ Separation *decreases*. For example, when beta1 is 0.08, increasing $B$ from 0.6 to 1.0 reduces the separation from 0.750 to 0.600. This indicates that stronger cross-phase modulation leads to less separation between the $U$ and $V$ solitons.

❖ **Max** ***U*****-*****V*** **Separation:**

This column quantifies the maximum temporal separation observed between the $U$ and $V$ solitons during their propagation. The values range from 0.400 to 0.750. The general trend observed from the table is that increasing either beta1 or $B$ (or both) leads to a *decrease* in the maximum $U$-$V$ separation. This suggests that both higher linear birefringence and stronger cross-phase modulation tend to reduce the maximum separation between the two polarization components。

**Key Findings:**

- The birefringence effect of the fiber causes the two polarization components to propagate at different group velocities, resulting in separation between the $U$ and $V$ solitons.
- Cross-phase modulation (parameter $B$) affects the interaction between the components.

## 5. Conclusion

This work aimed to study the nonlinear propagation of coupled pulses in birefringent optical fibers. But facing the difficulty of going through a direct integration method to obtain the solutions of the coupled nonlinear partial differential equation that governs the dynamics of waves in these waveguides, the iB-function was chosen to build the solution. Once this choice was made, the form of the solution to be constructed was specified. At this level, some calculations were done, which allowed the identification of the range of possible solutions, essentially outlining a domain where solutions could be found. While not all pairs within this range resulted in non-trivial solutions, we believe that most existing solutions can be located there. The challenge lies in the patience required to verify the existence of valid solutions. Analytical sequences were obtained that are solutions to the equations governing wave propagation in the birefringent fiber (dispersive and strongly nonlinear coupled Schrödinger equations). Finally, two families of solutions were found, which are the solitary waves and the trigonometric solutions for certain pairs, though not for all, as some pairs produced trivial solutions or even led to impossibilities. The principle used in this work was to adjust the properties of the fiber or waveguide to obtain coupled signals likely to propagate therein. Corresponding solutions were constructed numerically. The numerical solutions presented across the six cases obtained collectively illustrate the rich and diverse dynamics of coupled pulse propagation in birefringent optical fibers. They accurately capture complex

phenomena such as stable propagation of a coupled dark soliton with minimal walk-off, indicating strong interaction between the components(Case 1), energy exchange between the components during propagation which reveals instability in maintaining their coupled state (Cases 3, 5 and 6), to severe pulse broadening and breakdown at high intensities (Cases 2, 3 and 4), and modulational instability, providing invaluable insights into the behavior of light in such nonlinear waveguides under various conditions, all influenced by the fiber's birefringence and the initial pulse characteristics. This analysis could still consider higher-order dispersive effects or signal noise, which would provide additional information about the coupled pulse propagation. The consistency of these numerical observations with established theoretical solutions for these nonlinear optical effects enabled the validation of the accuracy of the numerical models employed. Moreover, a parametric study of the effect of birefringence parameters on soliton behaviour suggests that both higher linear birefringence parameter (beta 1) and stronger cross-phase modulation parameter ($B$) tend to reduce the maximum separation between the two polarization components, which is a strong indicator of group velocities walk-off. Walk-off can be a significant issue in optical communication systems, leading to pulse broadening if not properly managed. Regarding these results, we can confirm that our goal has been very well achieved because now it is easy for us to know exactly what types of signals we can use as propagating signal in birefringent optical fiber. A key recommendation from this work is to focus specifically on the manufacturing of optical fibers while considering the types of signals that can be best accommodated.

## Funding

This research paper does not receive funding from any organization.

## Acknowledgements

All authors approved the version of the manuscript to be published.

## Data Availability Statement

All data that support the findings of this study are included within the article.

## Authors' Contributions

J. R. Bogning: Conception of the project, writing, printing, investigation, computation and numerical study, interpretation of results. M. Fomekong: Execution of the project, writing, printing, investigation, computation and numerical study, interpretation of results. M. N. Zambo Abou'o: Investigation, writing, printing, computation, verification of results. O. L. Ndichia: Writing, printing, investigation, computation, verification of results.

## Conflicts of Interest

The authors declare no conflicts of interest regarding the publication of this paper.

## References


[1] Paliwal, D.R. (2025) Optical Fiber Communication. *International Journal of Scientific Research in Engineering and Management*, **9**, 1-9. https://doi.org/10.55041/ijsrem47650

[2] Mandeep, S., Debanuj, C., Suchita, Y., Sugeet, S., Karamdeep, S., Mrudula, K., Deepa, M.S.A., *et al*. (2024) Advancements in Optical Communication Research: A Review of India's Progress. *IEEE Photonics Journal*, **99**, 1-9.

[3] Salama, R. and Al-Turjman, F. (2024) An Overview of Long-Distance Optical Fiber Communication. *Journal of Biomedical Research & Environmental Sciences*, **5**, 1306-1312. https://doi.org/10.37871/jbres2018

[4] Agrawal, G.P. (2016) Optical Communication: Its History and Recent Progress. In: Al-Amri, M., El-Gomati, M. and Zubairy, M. Eds., *Optics in Our Time*, Springer International Publishing, 177-199. https://doi.org/10.1007/978-3-319-31903-2_8

[5] Khan, M.H.R. and Yesmin, L. (2001) Optical Fiber-Past, Present and Future: A Review. *Khulna University Studies*, **3**, 1-10.

[6] Zhao, Z. (2011) Past, Present and Future of Optical Fiber Communications. *Acta Optica Sinica*, **31**, Article ID: 0900109. https://doi.org/10.3788/aos201131.0900109

[7] Alsharari, M., Aliqab, K., Ali, F. and Armghan, A. (2023) Integrated Free-Space Optics and Fiber Optic Network Performance Enhancement for Sustaining 5G High Capacity Communications. *International Journal of Optics*, **2023**, Article ID: 8685686. https://doi.org/10.1155/2023/8685686

[8] Du, Y., Hu, G. and Bai, S. (2014) High Power All-Optical Gain-Clamped and Gain-Flattened Fiber Amplifier. *Chinese Journal of Lasers*, **41**, Article ID: 1205003. https://doi.org/10.3788/cjl201441.1205003

[9] Ming-Jun, L. (2020) Optical Fiber Evolution Over the Past 5 Decades. Frontiers in Optics/Laser Science, OSA Technical Digest (Optica Publishing Group).

[10] Motoharu, M. (2024) High-Power Optical Fiber Transmission Technologies for Radio-over-Fiber Networks. *IEICE Transactions on Communications*, **99**, 1-11.

[11] Zhong, Z.J., Liu, G.D., Yu, Y. and Chen, C. (2013) The High-Speed Video Signals Fiber Transmission Design Using of Optical Fiber in Photoelectric Tracking Equipment. *Advanced Materials Research*, **760**, 298-301. https://doi.org/10.4028/www.scientific.net/amr.760-762.298

[12] Pant, D., Malik, D. and Dudeja, D. (2014) Recent Progress in Fiber-Optic Communication. *Journal of Advance Research in Electrical & Electronics Engineering*, **1**, 6-9. https://doi.org/10.53555/nneee.v1i3.250

[13] Rottwitt, K. and Stentz, A.J. (2002) Raman Amplification in Lightwave Communication Systems. In: Kaminow, I.P. and Li, T., Eds., *Optical Fiber Telecommunications IV-A*, Elsevier, 213-257. https://doi.org/10.1016/b978-012395172-4/50005-x

[14] Liu, Y., Qi, Y., Cai, Y., Bao, X. and Gao, S. (2025) Recent Advances in Optical Fiber-Based Gas Sensors Utilizing Light-Induced Acoustic/Elastic Techniques. *Photoacoutics*, **43**, Article ID: 100715. https://doi.org/10.1016/j.pacs.2025.100715

[15] Winzer, P.G. (2012) High-Capacity Optical Transmission: Moving towards Shannon's Limit. *IEEE Photonics Journal*, **4**, 157-167.

[16] Taylor, J.R. (1996) Optical Solitons Theory and Experiment. *Optical Engineering*, **35**, 2437-2439. https://doi.org/10.1117/1.600816

[17] Wurster, L.M. and Ginner, L. (2018) Endoscopic Optical Coherence Tomography with a Flexible Fiber Bundle. *Journal of Biomedical Optics*, **23**, Article ID: 066001.

https://doi.org/10.1117/1.jbo.23.6.066001

[18] Ochoa, M., Algorri, J.F., Roldán-Varona, P., Rodríguez-Cobo, L. and López-Higuera, J.M. (2021) Recent Advances in Biomedical Photonic Sensors: A Focus on Optical-Fibre-Based Sensing. *Sensors*, **21**, Article 6469. https://doi.org/10.3390/s21196469

[19] Gu, R.Y., Mahalati, R.N. and Kahn, J.M. (2015) Design of Flexible Multi-Mode Fiber Endoscope. *Optics Express*, **23**, 26905-26918. https://doi.org/10.1364/oe.23.026905

[20] Wu, G., Zhu, R., Lu, Y., Hong, M. and Xu, F. (2024) Optical Scanning Endoscope via a Single Multimode Optical Fiber. *Opto-Electronic Science*, **3**, Article ID: 230041. https://doi.org/10.29026/oes.2024.230041

[21] Choksi, N. and Qian, L. (2024) Vector Theory of Optical Nonlinearities in Birefringent Fibers. *Journal of Lightwave Technology*, **42**, 1-12.

[22] Kumar, D.R. and Rao, B.P. (2012) Soliton Interaction in Birefringent Optical Fibers: Effects of Nonlinear Gain Devices. *Optik*, **123**, 117-124. https://doi.org/10.1016/j.ijleo.2011.03.009

[23] Ahmed, K.K., Alsahafi, N.A., Ahmed, H.M., Boulaaras, S. and Osman, M.S. (2025) Diverse Solitons Wave Structures for Coupled NLSEs in Birefringent Fibers with Higher Nonlinearities Using the Modified Extended Mapping Algorithm. *Scientific Reports*, **15**, Article No. 17047. https://doi.org/10.1038/s41598-025-00668-1

[24] Lakshmanan, M., Kanna, T. and Radhakrishnan, R. (2000) Shape-Changing Collisions of Coupled Bright Solitons in Birefringent Optical Fibers. *Reports on Mathematical Physics*, **46**, 143-156. https://doi.org/10.1016/s0034-4877(01)80018-5

[25] Lozano-Crisostomo, N., Garcia-Melgarejo, J.C., Gomez-Correa, J.E., Gonzalez-Galicia, M.A. and Villegas-Martinez, B.M. (2023) Polarization Coherence Theorem in Birefringent Nonlinear Single-Mode Optical Fibers. *Journal of Lightwave Technology*, **41**, 320-326. https://doi.org/10.1109/jlt.2022.3213486

[26] Tan, Z., Chen, X., Liu, N., Xu, J., Zhang, J., Zhu, Z., *et al.* (2024) Spatio-Temporal Nonlinear Theory in Birefringent Microrings. *Laser & Photonics Reviews*, **18**, Article ID: 2301281. https://doi.org/10.1002/lpor.202301281

[27] Yomba, E. and Ramchandra Nair, P. (2024) New Coupled Optical Solitons to Birefringent Fibers for Complex Ginzburg-Landau Equations with Hamiltonian Perturbations and Kerr Law Nonlinearity. *Mathematics*, **12**, Article 3073. https://doi.org/10.3390/math12193073

[28] Balla, P. and Agrawal, G.P. (2018) Nonlinear Interaction of Vector Solitons inside Birefringent Optical Fibers. *Physical Review A*, **98**, Article ID: 023822. https://doi.org/10.1103/physreva.98.023822

[29] Liu, J., Yi, Y. and Xu, T. (2025) Coupled-Mode Theory for Cross-Polarization Coupling in Optical Fibers. *Journal of Lightwave Technology*, **43**, 1-10.

[30] Jiang, Y., Tian, B., Liu, W., Sun, K. and Wang, P. (2013) Mixed-Type Solitons for the Coupled Higher-Order Nonlinear Schrödinger Equations in Multi-Mode and Birefringent Fibers. *Journal of Modern Optics*, **60**, 629-636. https://doi.org/10.1080/09500340.2013.798432

[31] Bogning, J.R., Abou'ou, M.N.Z., Tchinda, C.R.N., Fomekong, M., Ndichia, O.L., Songna, S.M., *et al.* (2024) Influence of Waveguide Properties on Wave Prototypes Likely to Accompany the Dynamics of Four-Wave Mixing in Optical Fibers. *Journal of Applied Mathematics and Physics*, **12**, 2601-2633. https://doi.org/10.4236/jamp.2024.127155

[32] Bogning, J.R. and Tchinda, C.N. (2021) Impact of the Properties of the Elliptical Birefringent Optical Fiber on the Nature and Propagation of Wave and Solitary Wave Solutions. *International Journal of Scientific Engineering and Science*, **5**, 27-43.

[33] Bogning, J.R. (2019) Mathematics for Nonlinear Physics: Solitary Wave in the Center of the Resolution of Dispersive Nonlinear Partial Differential Equations. USA Dorrance Publishing Co.

[34] Bogning, J.R., Djeumen Tchaho, C. and Kofané, T. (2012) Generalization of the Bogning-Djeumen Tchaho-Kofané Method for the Construction of the Solitary Waves and the Survey of the Instabilities. *Far East Journal of Dynamical Systems*, **20**, 101-119.

[35] Ngouo Tchinda, C. and Roger Bogning, J. (2020) Solitary Waves and Property Management of Nonlinear Dispersive and Flattened Optical Fiber. *American Journal of Optics and Photonics*, **8**, 27-43. https://doi.org/10.11648/j.ajop.20200801.13